TP4225E

A MATHEMATICAL ANALYSIS OF DYNAMIC ICE RUPTURE BY HOVERCRAFT.

Prepared for the
Transport Development Centre
Transport Canada
March 1983

CA1
DTC 847
83
M11
c.2

Colombret, Inc.

85-2367/

TP 4235E

A MATHEMATICAL ANALYSIS OF DYNAMIC ICE RUPTURE BY HOVERCRAFT

by

Marvin Shinbrot, F.R.S.C.
M. Shinbrot, Inc.
1140 Oscar Street
Victoria, B.C. V8V 2X4

March 1983

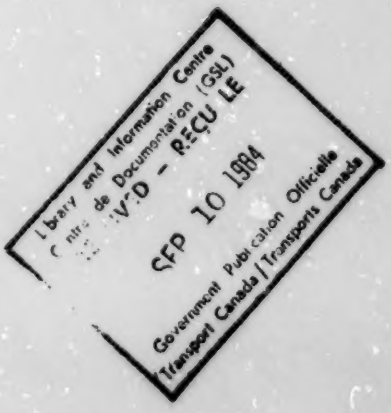

The content of this report reflects the views of the contractor and not necessarily the official views or policies of the Transportation Development Centre of Transport Canada.

REPORT DOCUMENTATION FORM

1. Transport Canada Report No.	2. TDC Project No.	3. Recipient's Catalogue No.
TP 4235 E	4297	

4. Title and Subtitle	5. Report Date
A Mathematical Analysis of Dynamic Ice Rupture by Hovercraft.	March 1983
	6. Performing Organization Report No.
7. Author(s)	8. Transport Canada File No.
Dr. Marvin Shinbrot, F.R.S.C.	D1460-151-1
9. Performing Organization Name and Address	10. DSS File No.
M. Shinbrot Mathematical Consulting, Inc. 1140 Oscar Street Victoria, B.C. V8V 2X4	T-8200-0-00540
	11. DSS or Transport Canada Contract No.
	OS DB1-00076
12. Sponsoring Agency Name and Address	13. Type of Report and Period Covered
Transportation Development Centre (TDC) 1000 Sherbrooke Street West, Suite 2421 Montreal, Quebec H3A 2R3	Final Report, Aug. 81-Mar. 83
	14. Sponsoring Agency Code
	4297
15. Supplementary Notes	16. TDC Project Officer
	J.E. Laframboise

17. Abstract

A theory of the motion and eventual rupture of ice by hovercraft is presented. It is shown that the theory predicts details of the ice motion that have been observed in the field and that have not been predicted by any other theory. It is also shown that it may be feasible to design an optimal hovercraft for icebreaking purposes using the methods described here.

18. Key Words	19. Distribution Statement
Icebreaking, hovercraft, dynamic rupture, ice, mathematical analysis	Limited number of copies available at TDC.

20. Security Classification (of this report)	21. Security Classification (of this page)	22. No. of Pages	23. Price
none	none	47	

TDC/CDT 79-005

FORMULE DE DOCUMENTATION POUR RAPPORT

1. N° du rapport Transports Canada	2. N° de l'étude — CDT	3. N° de catalogue du destinataire
TP 4235 E	4297	

4. Titre et sous-titre	5. Date du rapport
A Mathematical Analysis of Dynamic Ice Rupture by Hovercraft	Mars 1983
	6. N° du rapport de l'organisme exécutant

7. Auteur(s)	8. N° de dossier Transports Canada
Dr. Marvin Shinbrot, F.R.S.C.	D1460-151-1

9. Nom et adresse de l'organisme exécutant	10. N° de dossier — ASC
M. Shinbrot Mathematical Consulting Inc. 1140 rue Oscar Victoria, B.C. V8V 2X4	T8200-0-00540
	11. N° de contrat — ASC ou Transports Canada OS DB1-00076

12. Nom et adresse de l'organisme parrain	13. Genre de rapport et période visée
Centre de développement des transports (CDT) 1,000 ouest rue Sherbrooke, suite 2421 Montréal, Québec H3A 2R3	Rapport final, août 81 - mars 83
	14. Code de l'organisme parrain 4297

15. Remarques additionnelles	16. Agent de projet — CDT
	J.E. Laframboise

17. Résumé

Une théorie du déplacement et du bris éventuel des glaces par un aéroglisseur fait l'objet de la présentation. Il est montré que cette théorie permet de prévoir avec précision les déplacements des glaces tels qu'ils ont pu être observés dans la réalité, alors qu'aucune autre théorie n'a pu les prévoir. Il est également montré qu'il est possible de mettre au point un aéroglisseur capable de briser la glace en utilisant les méthodes ci-après décrites.

18. Mots-clés	19. Diffusion
Brise-glace, aéroglisseurs, Rupture dynamique, glace, analyse mathematique	nobre limité de copies disposibles au CDT

20. Classification de sécurité (de ce rapport)	21. Classification de sécurité (de cette page)	22. Nombre de pages	23. Prix
aucune	aucune	47	—

CDT 7DC 79-005

PROJECT TEAM

The project team for M. Shinbrot, Inc. was composed of:

Dr. Marvin Shinbrot, F.R.S.C.
Dr. John Reeder

TABLE OF CONTENTS

1.	INTRODUCTION	p. 1
2.	THE NEVEL THEORY	3
3.	PRELIMINARY RESULTS	5
	3.1 Introductory	5
	3.2 Onset of High Speed Motion	5
	3.3 The Wave Pattern	7
	3.4 Ice Displacement	19
4.	RECTANGULAR VEHICLE	21
	4.1 Ice Displacement	21
	4.2 Stresses Behind the Vehicle	23
5.	CONCLUSIONS	25
6.	REFERENCES	26
Appendix A.	The Dispersion Relation	27
Appendix B.	Nevel's solution	29
Appendix C.	The Impulse Response	32
Appendix D.	The Response to a Moving Impulse	33
Appendix E.	Equations for the Wave Pattern	35
Appendix F.	Steady Ice Displacement Due to a Moving Impulse	39
Appendix G.	The Rectangular Vehicle	44

LIST OF FIGURES

Figure 1.	Geometry of Wave Motion	p. 5
Figure 2.	Onset of High Speed Operation	6
Figure 3.	The Wave Pattern, h = 0	9
Figure 4.	The Wave Pattern, h = .001, U = 10	10
Figure 5.	The Wave Pattern, h = .01, U = 10	11
Figure 6.	The Wave Pattern, h = .05, U = 10	12
Figure 7.	The Wave Pattern, h = .1, U = 10	13
Figure 8.	The Wave Pattern, h = .1, U = 15	14
Figure 9.	The Wave Pattern, h = .05, U = 7.5	15
Figure 10.	The Wave Pattern, h = .05, U = 20	16
Figure 11.	Angle of Radial Crests vs. h.	17
Figure 12.	Angle of Radial Crests vs. U.	18
Figure 13.	Ice Displacement Behind Point Vehicle.	20
Figure 14.	Ice Displacement Behind Rectangular Vehicle.	22
Figure 15.	Relative Stress in the Hump Wave.	24

TABLE 1 List of Symbols

a	Half-length of ACV.
A	Area of ACV.
b	Half-width of vehicle.
$c(k)$	Wave speed.
$c_0(\kappa)$	Dimensionless wave speed: $c_0(\kappa) = c(k)\sqrt{\frac{\varepsilon}{\mu g h}}$.
$C(k)$	Group velocity.
D	$Eh^3/12(1-\sigma^2)$
D_0	$D/\rho g h^4$
E	Young's modulus for ice. (Always taken to be 3×10^9 Pa.)
F	$\varepsilon U^2/\mu g h$
$\hat{f}$	Fourier transform of the function f: $\hat{f}(\underline{k}) = \int_{-\infty}^{\infty}\int_{-\infty}^{\infty} f(\underline{x})e^{i\underline{k}\cdot\underline{x}}\,dx\,dz.$
g	Acceleration due to gravity.
h	Thickness of ice, assumed constant.
i	$\sqrt{-1}$
$\underline{k} = (k_1,k_2)$	Vector wave number.
k	$\lvert\underline{k}\rvert$
p	Pressure in water.
P	Pressure distribution on the ice.
P_0	Cushion pressure under ACV, assumed constant.
R	C/c.
r	$\lvert\underline{x}\rvert = \sqrt{x^2+z^2}$.
t	Time.
U	Speed of ACV, assumed constant.
U_0	Minimum speed of high speed operation.
V	Vertical force on the ice.
v_{crit}	Critical velocity according to Nevel.
w	Dispersion relation in moving coordinates: $w = Uk_1 + \omega$.
$\underline{x} = (x,z)$	Position vector in the ice.
$\tilde{x}$	$\varepsilon F^{1/3}x/\mu h$.
y	Vertical distance, measured upward from the equilibrium position of the ice.
α	Aspect ratio of ACV, $\alpha = a/b$.
δ	Small positive number.

∇	$(\partial/\partial x, \partial/\partial z)$.
ϵ	$\mu/D_0^{1/4}$.
θ	Phase angle.
θ_0	Asymptotic angle made by radial crests with direction of ACV.
κ	$\mu kh/\epsilon$.
λ	$(F\cos^2\psi)^{1/3}$
μ	ρ'/ρ. (Always taken to be 0.9.)
ρ	Density of water.
ρ'	Density of ice.
σ	Poisson's ratio for ice. (Always taken to be 1/3.)
ξ	$x(\epsilon\sqrt{F}/\mu h)$
η	Ice displacement
η_0	Ice displacement due to instantaneous impulse.
η_R	$\eta\left[\dfrac{3\pi\epsilon^2\rho g F^{4/3}}{2\mu^2 h^2 p_0}\right]$
η_s	$\eta(\rho g F^{2/3})$.
ζ	$z(\epsilon\sqrt{F}/\mu h)$.
ϕ	Velocity potential in the water.
χ	Polar angle in $\underline{x}$-plane.
ψ	Polar angle in $\underline{k}$-plane.
$\omega(k)$	Dispersion relation.
$\omega_0(\kappa)$	Dimensionless dispersion relation: $\sqrt{\dfrac{\kappa(1+\kappa^4)}{1+\epsilon\kappa}}$

Literal subscripts always mean differentiation. Thus, e.g. $\phi_y = \partial\phi/\partial y$.

1. INTRODUCTION

It goes without saying that icebreaking is an important endeavour in any northern country such as Canada, and any new method for breaking ice is deserving of study. Such a method was discovered some years ago, when an air cushion vehicle (ACV) was observed to break ice 27 inches thick while travelling about 4 mph. [1]. Since that time, ACVs have been used regularly as icebreakers, particularly in remote areas, inaccessible to conventional icebreakers.

In order to understand how ice is broken by a moving ACV, and also to be able to improve its performance, a theory is required. The first attempt at such a theory was made in the United States by Donald E. Nevel [2]. According to Nevel, there should be an optimum speed for an ACV to travel to maximize its effects on plate ice. For the vehicle to travel slower or faster than this critical velocity v_{crit} results in less efficient icebreaking. Since such velocity-dependent effects have been observed in the field, Nevel's theory has been received with much interest and attention.

On the other hand, Nevel's theory is paradoxical [3]. Not merely is the effectiveness of a vehicle maximized at the speed v_{crit}, but the displacement of the ice goes to infinity there, according to Nevel. What is more, v_{crit} does not depend in any way on the vehicle, not on its size, not on its weight. Thus, if Nevel's theory is correct, a mouse running across 10 metres of ice will immediately cause a very large displacement, contrary to all experience.

Nevel assumed that the ice can be treated as a plate. In attempting to overcome the paradox in Nevel's theory, it was proposed [3] in 1980 that the ice be treated instead as an isotropic, homogeneous medium (IHM), and it was shown that, when this is done, the "running mouse paradox" does not occur. Encouraged by this result, it was proposed to Transport Canada that a deeper study be made, treating this ice as an IHM, with the intention of proposing a more efficient vehicle for icebreaking. After all, the ACVs currently used to break ice are off-the-shelf vehicles, designed for other purposes entirely. It was suggested that there might be a vehicle with an optimum planform or other characteristics, designed specifically for breaking ice. To seek for an optimum vehicle using IHM theory was the original purpose of the project reported on here.

About halfway through the project, however, it was discovered that Nevel's theory is not merely paradoxical, but wrong. This understanding came about in the following way. Nevel's theory is paradoxical not merely because the ice displacement goes to infinity, but because, at the speed

v_{crit}, the theory implies that the ice cannot be touched so softly that it is not driven into the nonlinear range. This is the real meaning of the running mouse paradox. Thus, if Nevel's theory were correct, linearization itself is not valid at the speed v_{crit}. But if linear theory is not valid when a 15 gram mouse runs over 10 meters of ice, it is never valid. This understanding led to a closer look at Nevel's theory and, when this was done, it was found that Nevel had unintentionally drawn the wrong conclusion from his calculations.

At this point, a correct theory was formulated, in which ice is treated as a plate, as in Nevel. Using the new theory, it became possible to show immediately that the running mouse paradox no longer occurs, even in the framework of plate theory. Since the original proposal to study ice as an IHM was based on the belief that Nevel's mathematics were correct and therefore that plate theory leads inevitably to the running mouse paradox, with the permission of Transport Canada the proposal was changed to study the new theory. After all, considering the ice as an IHM is much more complicated than considering it as a plate. The new proposal then was made on the basis of the general scientific and sound engineering principle of never using a complicated model when a simple one will do.

This report, then, presents a valid theory of icebreaking, treating the ice as a plate. We begin with Nevel's theory and show why it is wrong. A correct theory is then presented. This theory leads at once to some new results: on the onset of high speed operation, on the possible occurrence of forward cracks in the ice, etc. These results, as well as a discussion of the wave patterns in the ice, are presented in §3.

Since the goal of this work was originally to present design criteria for an optimum vehicle for icebreaking, a step toward the goal is taken in §4. It was not possible to complete the analysis due to limitations of time, but, by considering the variation of stress in the ice as a function of aspect ratio, it is shown that such a goal is probably feasible. Further discussion of this can be found in §4 and in the Conclusions.

There are a number of hypotheses that go into our analysis. We discuss them here and then make them without further mention. The first, as we have already said, is that the ice can be treated as a thin plate of constant thickness. Second, it is assumed that the icefield is unbroken. The idea here is that it is probably easier to break up an icefield which is already partially broken than an intact one. Thus, we attempt to maximize the stresses in an unbroken field and assume that such stresses would also be effective in an ice field in which rupture has already begun. Finally, it is assumed that the water under the ice is deep. Further study should be made on the effects of water depth. (In this regard, see [1].)

2. THE NEVEL THEORY

In this part, we point out the mathematical mistake made by Nevel in [2]. The derivation of Nevel's results is to be found in appendices A and B.

According to Nevel, the Fourier transform of the displacement of the ice in response to a pressure distribution P moving with constant speed U along the negative x-axis is given by (B7). One assumption that goes into the derivation of (B7) is that the vehicle has been travelling along the ice for a long enough time that all transients have died out and the ice response is steady.

To look at a simple case, suppose the applied pressure P is a unit impulse. Then $\hat{P} = 1$, and, since $\rho\mu = \rho'$, (B7) gives

$$\hat{\eta} = \frac{k}{(\rho+\rho' hk)(U^2k_1^2-\omega^2)} . \tag{2.1}$$

Now, the ice response to an impulse that is not yet steady is derived in appendices C and D. The Fourier transform of the ice displacement at the time t after the vehicle has started to move is

$$\hat{\eta} = \frac{k}{z(\rho+\rho' hk)\omega(k)} \left[\frac{1-e^{it(Uk_1-\omega(k))}}{Uk_1-\omega(k)} - \frac{1-e^{it(Uk_1+\omega(k))}}{Uk_1+\omega(k)} \right] \tag{2.2}$$

(see equation (D2).

Equations (2.1) and (2.2) should not be compared directly, since (2.1) is the purported steady response, while (2.2) is the transient response of the ice. Notice that we may <u>not</u> let t go to infinity in (2.2) since the exponentials are both oscillatory and have no limit.

However, we may think of adding a damping term to the exponentials in order to force them to go to zero. If we do this, the result of letting t go to infinity in (2.2) will be

$$\hat{\eta} \to \frac{k}{2(\rho+\rho' kh)\omega(k)} \left[\frac{1}{Uk_1-\omega(k)} - \frac{1}{Uk_1+\omega(k)} \right]$$

$$= \frac{k}{(\rho+\rho' hk)(U^2k_1^2-\omega^2)} .$$

This is exactly Nevel's formula (2.1).

Thus, we see that Nevel's formula (2.1) is obtained from the correct formula (2.2) by introducing an artificial damping into (2.2) and sending t to infinity. But where did the damping come from? Is it necessary to introduce a damping, or have we lost something by doing so? To find out, we turn to the formula (D1) for the displacement at time t. It is

$$\eta = \int_0^t \eta_0 (\tau, x-U\tau, z)d\tau \ . \tag{2.3}$$

In this formula, we are allowed to send t to infinity to find the steady response, and the result is

$$\eta \to \int_0^\infty \eta_0 (\tau, x-U\tau, z)dz \ . \tag{2.4}$$

This is a perfectly well defined, convergent integral. Thus, the problem in [2] is this, that although there is a steady response that can be obtained from the transient response (2.3) by sending t to infinity, it is not permissible mathematically to send t to infinity in the formula (2.2) for the Fourier transform of the transient response. The difficulty is that the steady response (2.4) does not have a Fourier transform, since it does not go to zero fast enough at infinity.

This difficulty is a technical, mathematical one, that can be got around in several ways. One way, in fact, begins with Nevel's formula (2.1) and treats the zero of the denominator as a pole of the analytic function (2.1). The formula for η is then obtained from the formula for the inverse Fourier transform by indenting the path of integration into the upper or lower half-plane. This kind of indentation is discussed in some detail in the context of water waves by Lamb [4].

3. PRELIMINARY RESULTS

3.1 Introductory.

Knowing now that trying to solve the steady problem (B1)-(B5) directly by Fourier transforms leads to error, we seek a new method for solving the problem. The new method leads to immediate results, as will be seen.

3.2 The Onset of High Speed Motion.

When an ACV is stationary, of course no waves are produced on the ice, and the ice displacement is in the form of a symmetrical bowl. When the vehicle first begins to move, there are still no waves formed, the bowl remains, but it becomes asymmetrical fore and aft. When there are no waves on the ice, we say the vehicle is operating in the low speed mode. We are primarily interested in the high speed mode, when waves are formed, since it has often been observed that ice cracks in the first crest behind the vehicle (the "hump wave"). In this part, we calculate the speed at which high speed motion begins and analyze some of the wave patterns.

We consider a vehicle moving along the negative x-axis at a speed U. For now, we treat the vehicle as a moving pressure point. Consider the point moving from Q to P in Figure 1.

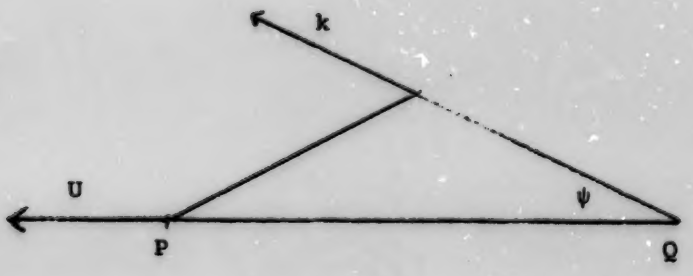

Figure 1. Geometry of Wave Motion

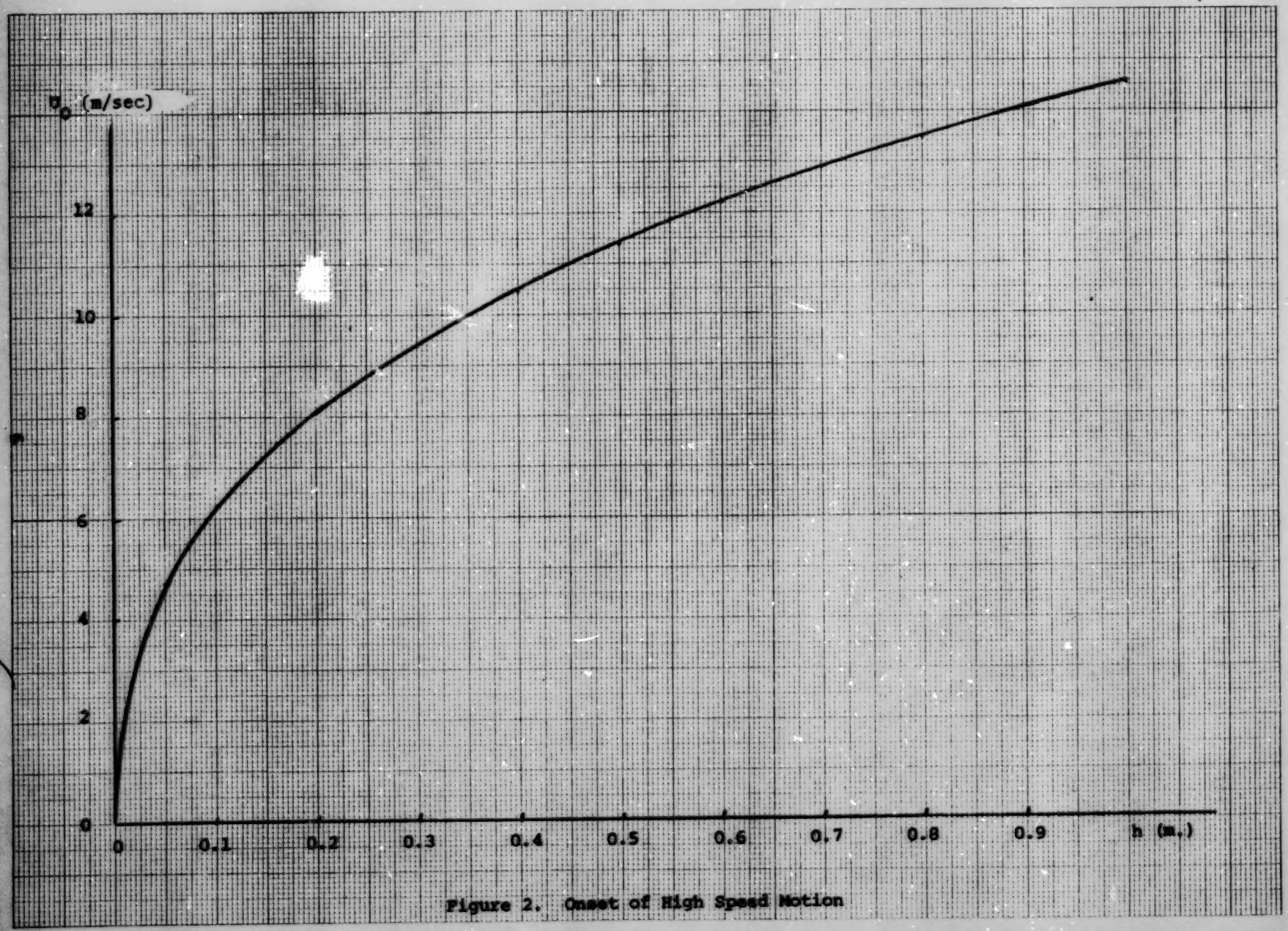

Figure 2. Onset of High Speed Motion

For a wave crest to keep up with the vehicle, we must have

$$U \cos \psi = c(k) \tag{3.1}$$

To see this, place the coordinate system in the ACV, and consider the ice as moving from left to right under it. The ice moves at speed U and has a component $U \cos \psi$ in the direction of $\underline{k}$. This must equal the wave speed associated with $\underline{k}$, which is what (3.1) says.

Now, $c(k)$ has a minimum. For (3.1) to be satisfied, then U may not be less than the minimum of $c(k)$. Thus, if we set

$$U_0 = \min_{k \geq 0} c(k),$$

then we must have $U \geq U_0$ in order for waves to appear. U_0, then, is the speed at which high speed operation begins. U_0 is a function of h and is plotted vs. h in Figure 2.

3.3 The Wave Pattern.

To understand how the ice breaks, it is necessary to understand how it deforms under the motion of the ACV. The first step in this understanding is the description of the wave pattern, as viewed from above, due to a moving pressure point. In this section, we describe the pattern.

Parametric equations for the wave pattern are derived in appendix E, where it is shown that these equations may be written, in dimensionless form,

$$\left.\begin{aligned} \xi &= \theta \cdot \frac{F - Rc_0^2}{\kappa c_0 (1-R)} \\ \zeta &= \theta \cdot \frac{R\sqrt{F - c_0^2}}{\kappa (1-R)} \end{aligned}\right\} \tag{3.2}$$

Our task now is to present graphs of these parametric equations for various values of the parameters U and h.

To begin the discussion, we consider the case $h = 0$. In that case, the parametric equations for the wave crests are given, not by (3.2), but by (E8). The wave pattern, viewed from above, is shown in Figure 3. This pattern in the pattern produced by a moving pressure point in water of infinite depth. Figure 3 is well known and can be found in any book on water waves (See, e.g., [4, 5, 6].)

Figure 3 is presented to point out that, as is easily seen, all the crests are similar. Also, they are symmetric about the x-axis. Thus, to

see the pattern it is enough to present one-half of one of the curves. (The heavy curve in Figure 3.) Since the properties of similarity and symmetry are retained in the ice patterns, when $h \neq 0$, and since, as we shall see, these patterns are a little complicated, in what follows, we only present one-half of one of the crests. The rest of the pattern can then easily be reconstructed.

The wave patterns on ice depend on h and U, and they are displayed for varying circumstances in figures 4 through 10, which we proceed to discuss.

Figures 4 through 7 show the effect of ice thickness on the pattern; all these figures are drawn for a vehicle moving at a constant speed U of 10 metres per second. The pattern for very thin ice is shown in figure 4. As can be seen, the curved portion of the wave crest is very similar to the heavy crest drawn in figure 13. (The radial crests appearing in figures 4 - 10 are discussed below.) Increasing h for fixed U has the effect of making the pattern less and less like that of water waves, until one arrives at the pattern of figure 7, which shows the pattern when $h = .01$ metres. Increasing h further continues to produce a pattern much like that of figure 7.

The effect of changing U is shown in figures 7 and 8, which show the pattern for the same value of h. As can be seen, increasing U moves the pattern closer to that of figure 3. This can also be seen by comparing figures 9, 6, and 10, which are drawn for a different value of h.

Notice that the experimentally observed hump wave is clearly to be seen in all the figures.

Also to be seen in figures 4 - 10 are the nearly straight radial crests opening to the left and the right. These are interesting because it has been observed that ice sometimes breaks, not in the hump wave, but in radial cracks shooting forward from the ACV. These observed cracks may well be produced by the radial crests shown in figures 4 - 10. To decide this question, further work is needed to calculate the stresses in the radial crests. However, we point out that the present theory is the first to offer any explanation of the phenomenon of radial cracking.

Because these radial crests are of some interest, we present a little more detail of them in figures 11 and 12, which show, as functions of h and of U, the angle θ_0 made by the radial crests with the x-axis. (See figure 5 for a definition of θ_0.) As radial cracks, when they occur, are rather sharp and clearly defined, figures 11 and 12 may be useful in providing a verification of the theory.

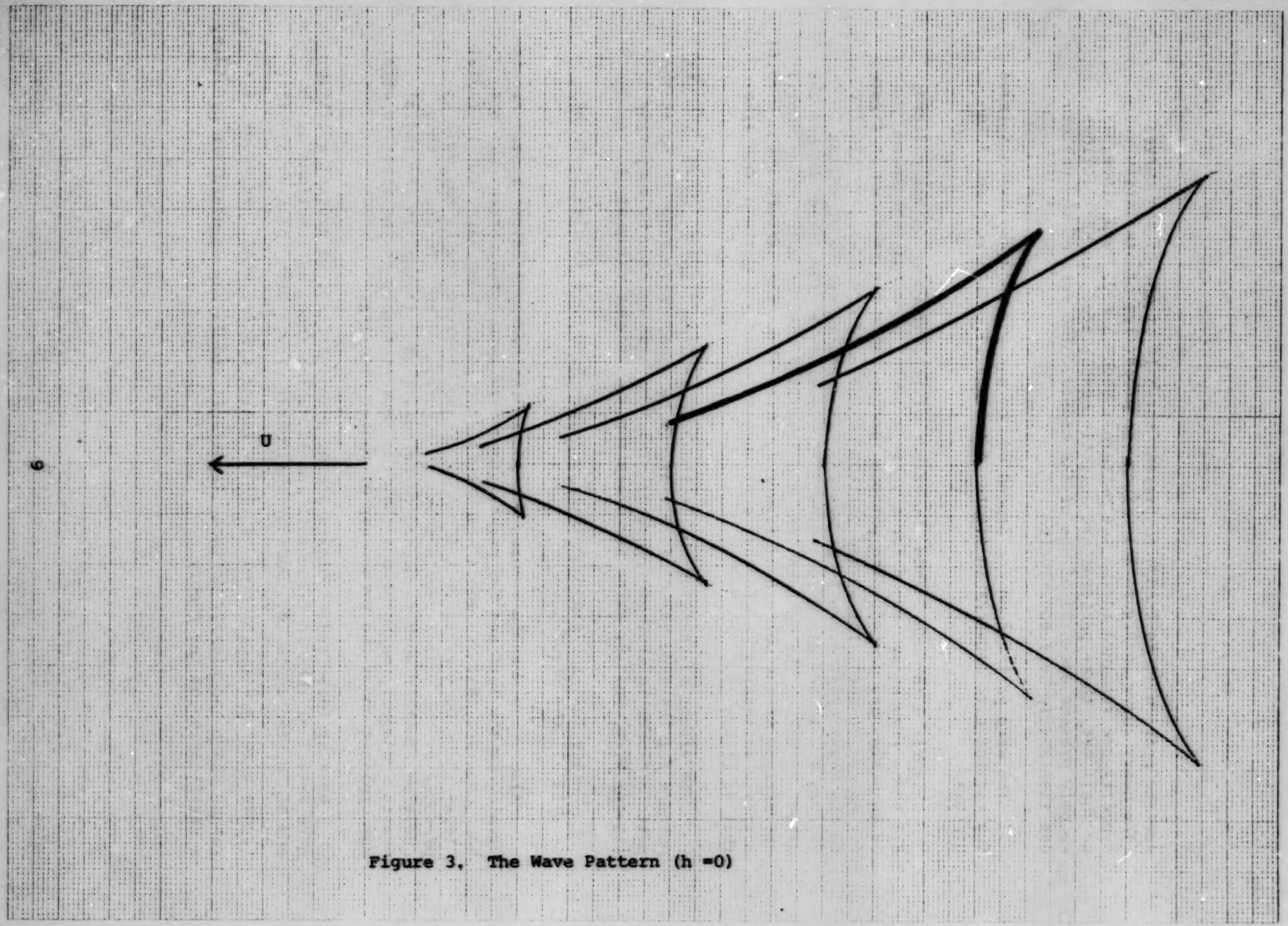

Figure 3. The Wave Pattern (h =0)

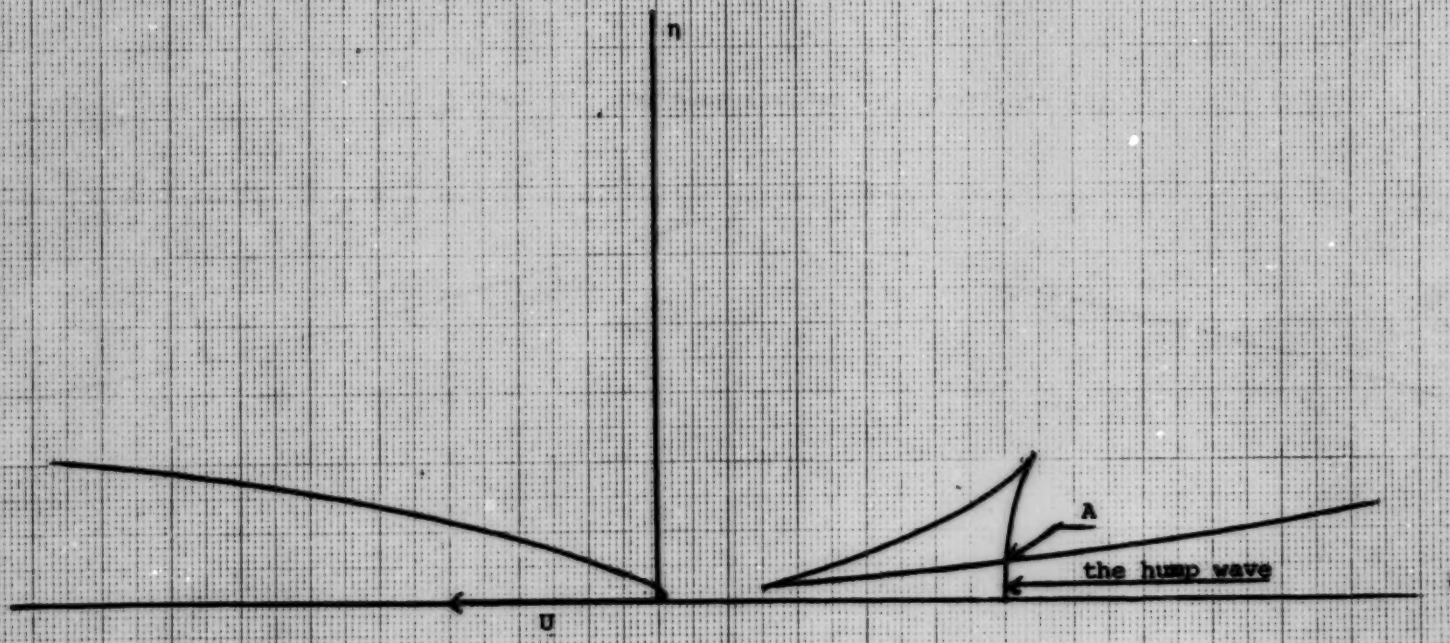

Figure 4. The Wave Pattern (h =.001, U = 10)

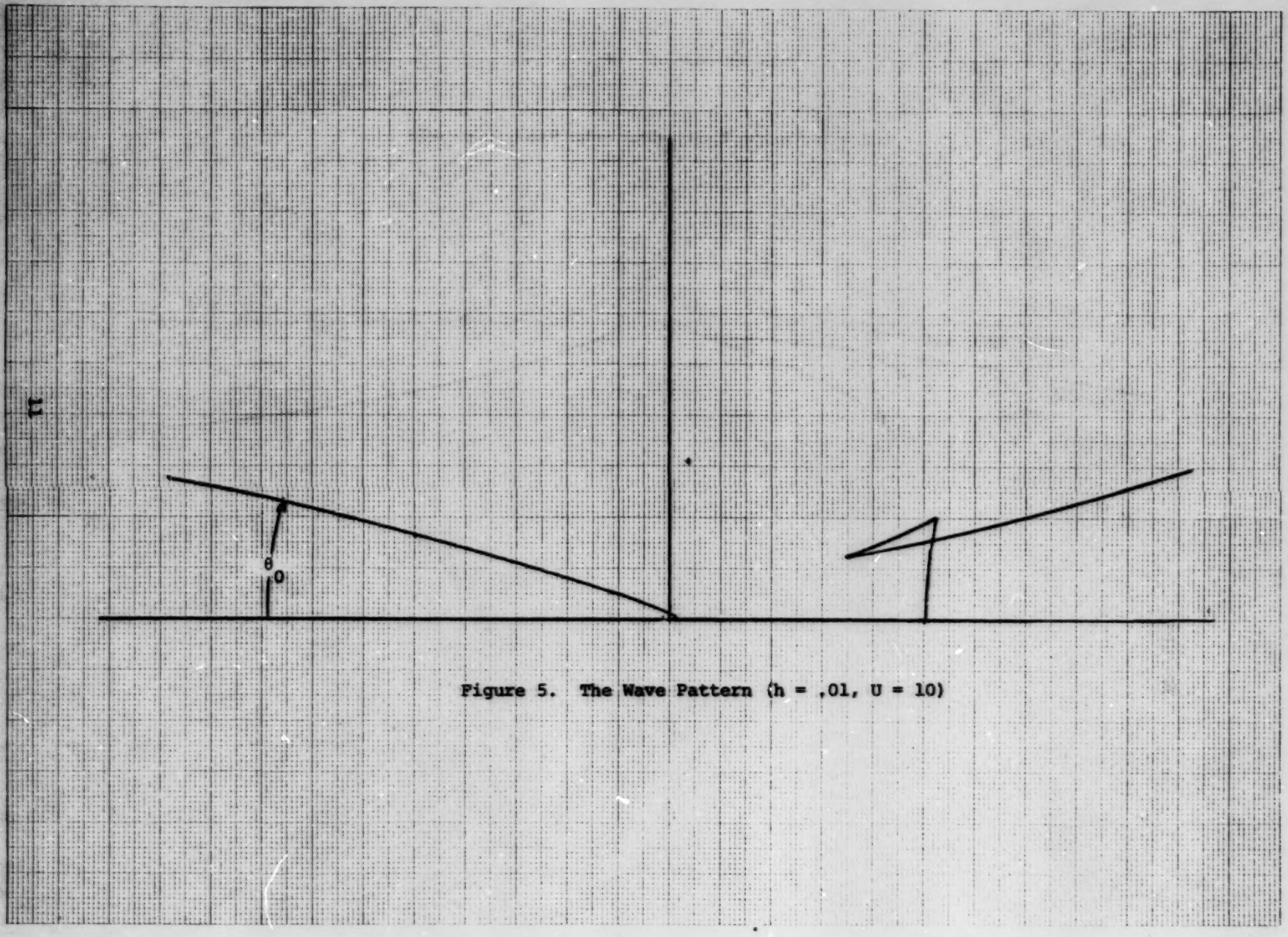

Figure 5. The Wave Pattern (h = ,01, U = 10)

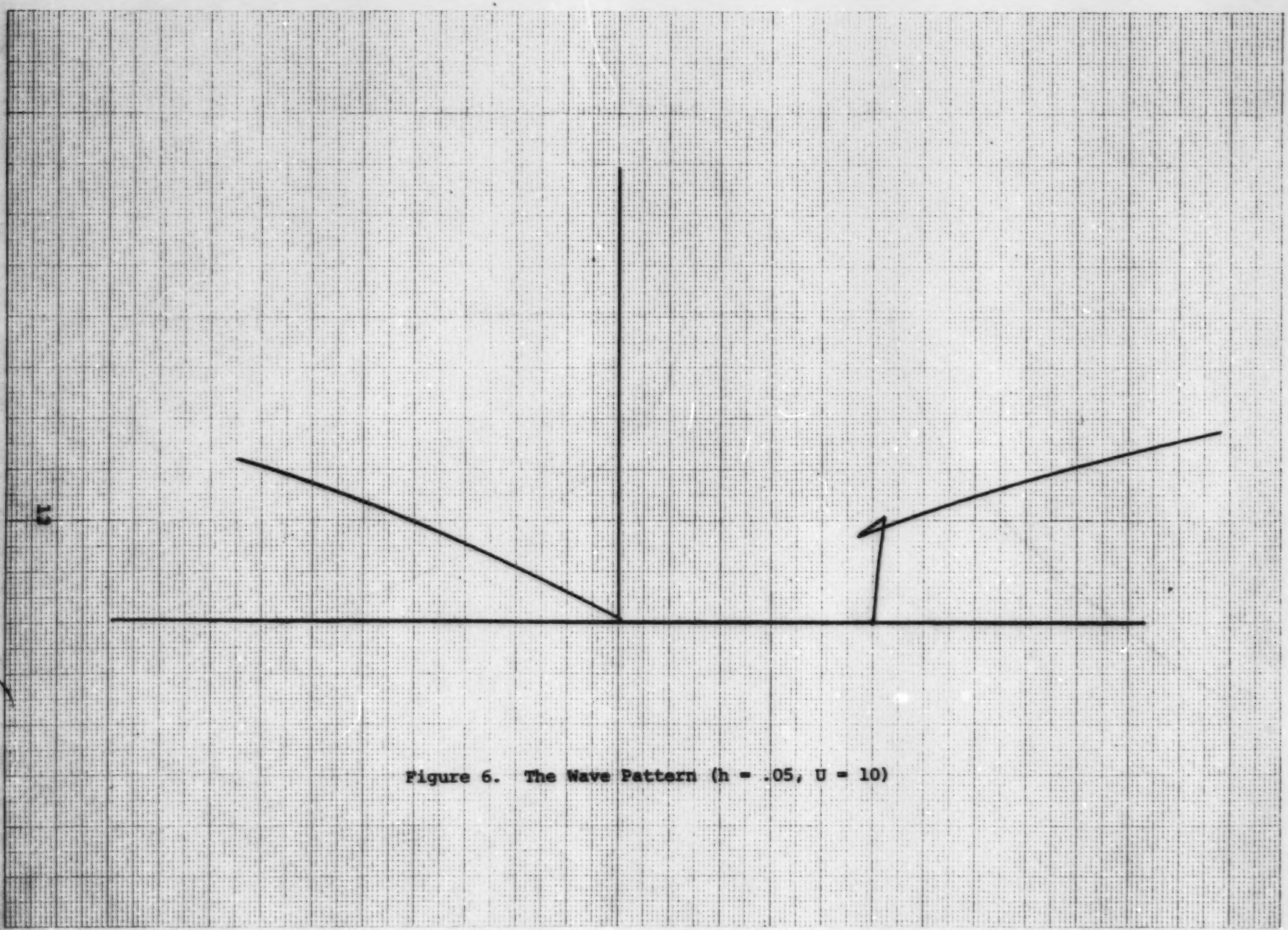

Figure 6. The Wave Pattern (h = .05, U = 10)

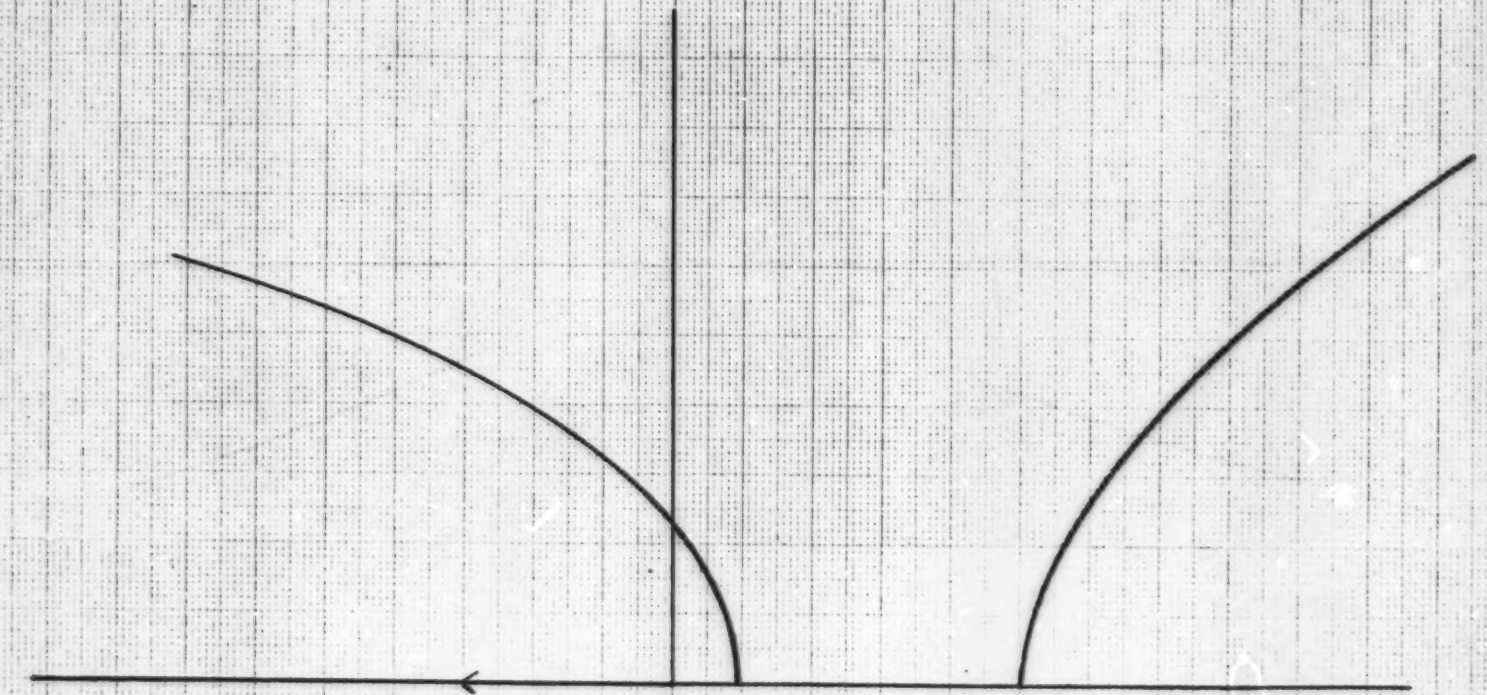

Figure 7. The Wave Pattern (h = .1, U = 10)

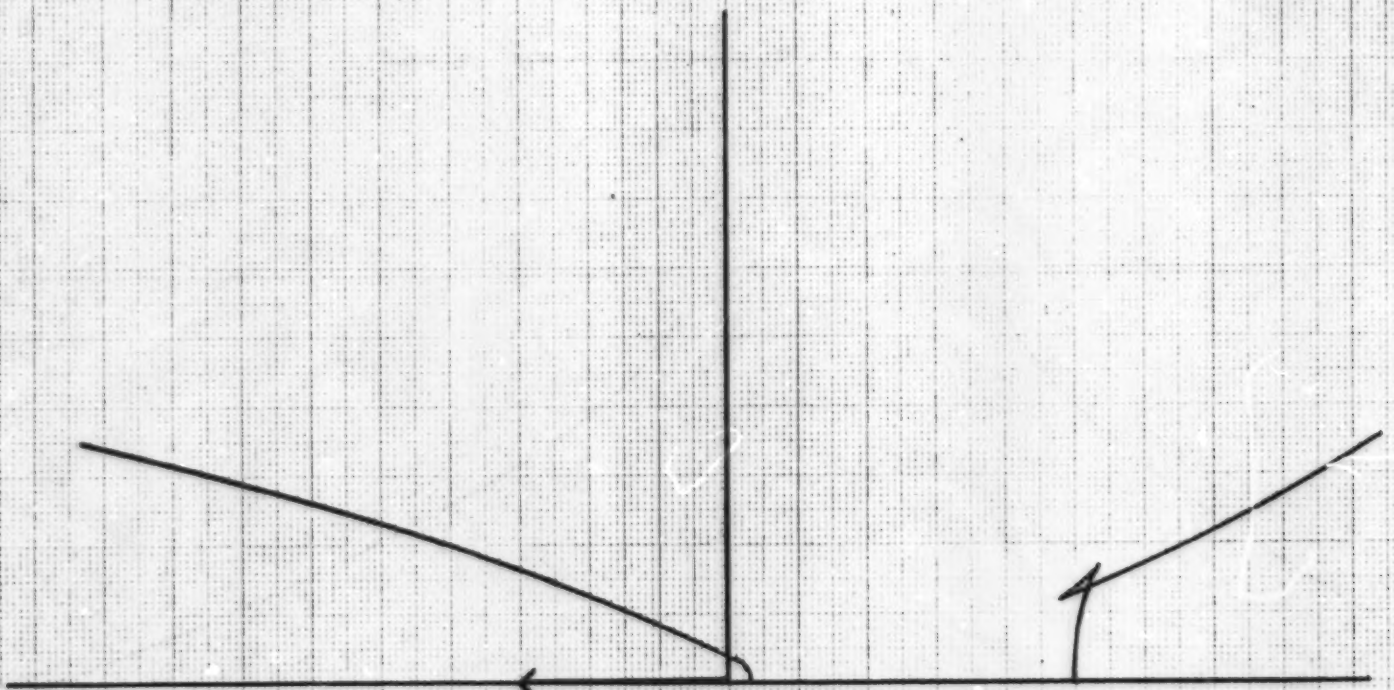

Figure 8. The Wave Pattern (h = .1, U = 15)

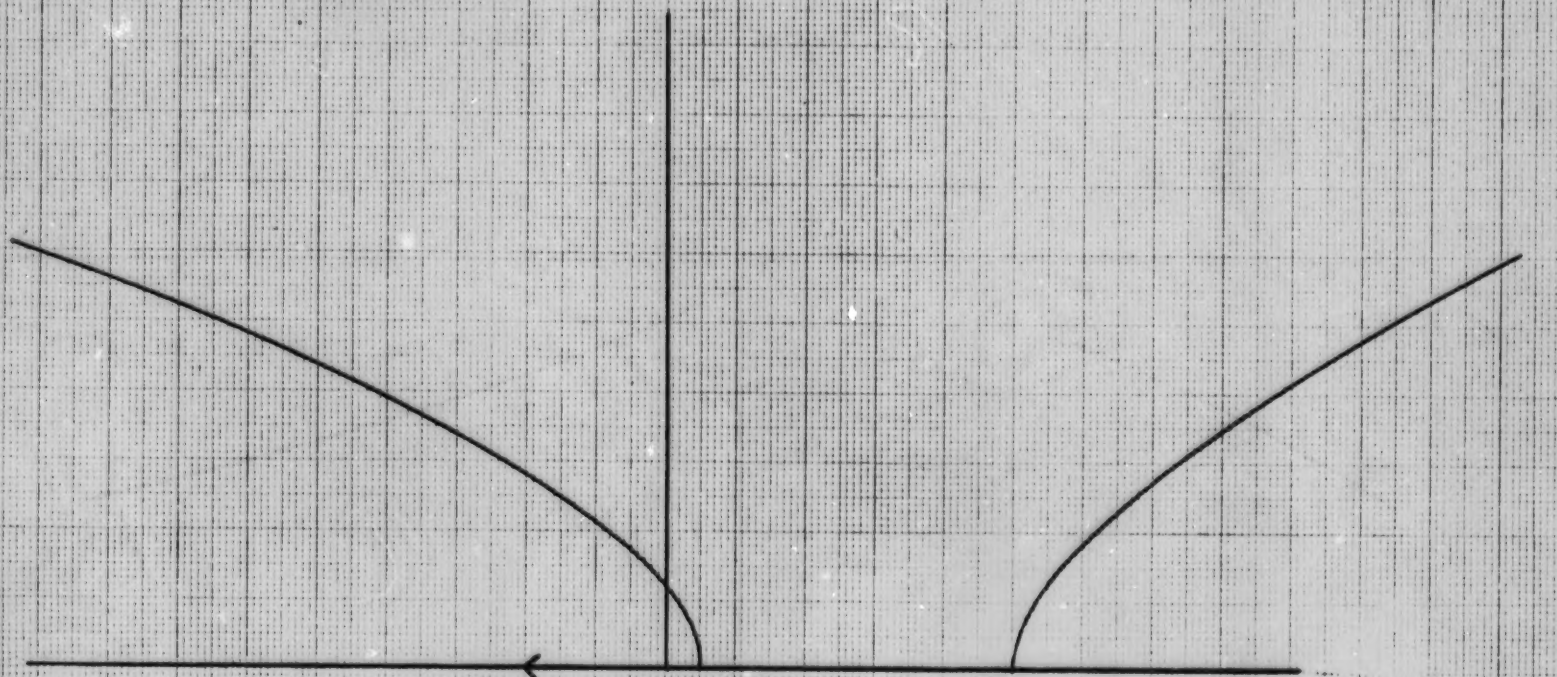

Figure 9. The Wave Pattern (h = .05, U = 7.5)

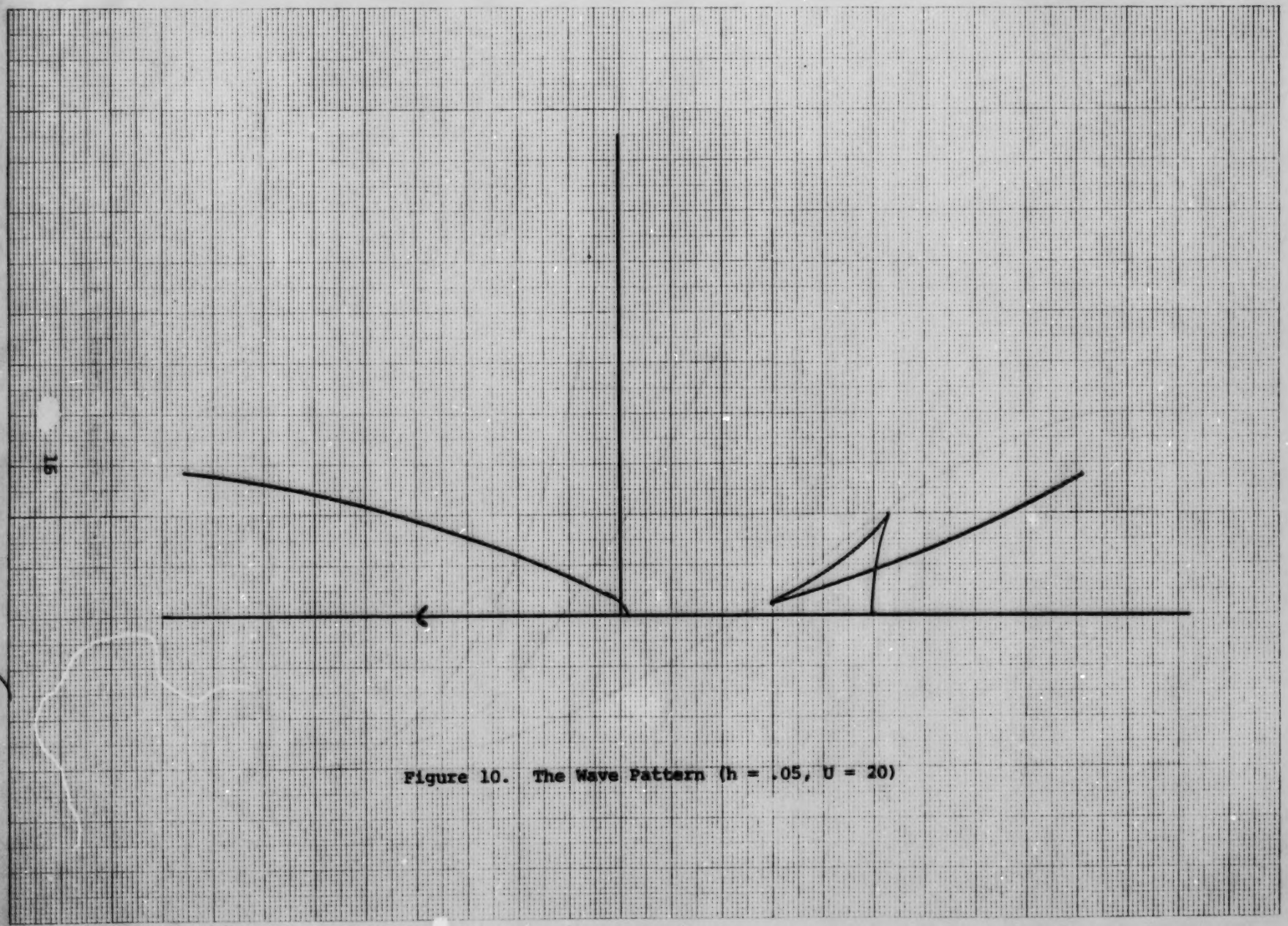

Figure 10. The Wave Pattern (h = .05, U = 20)

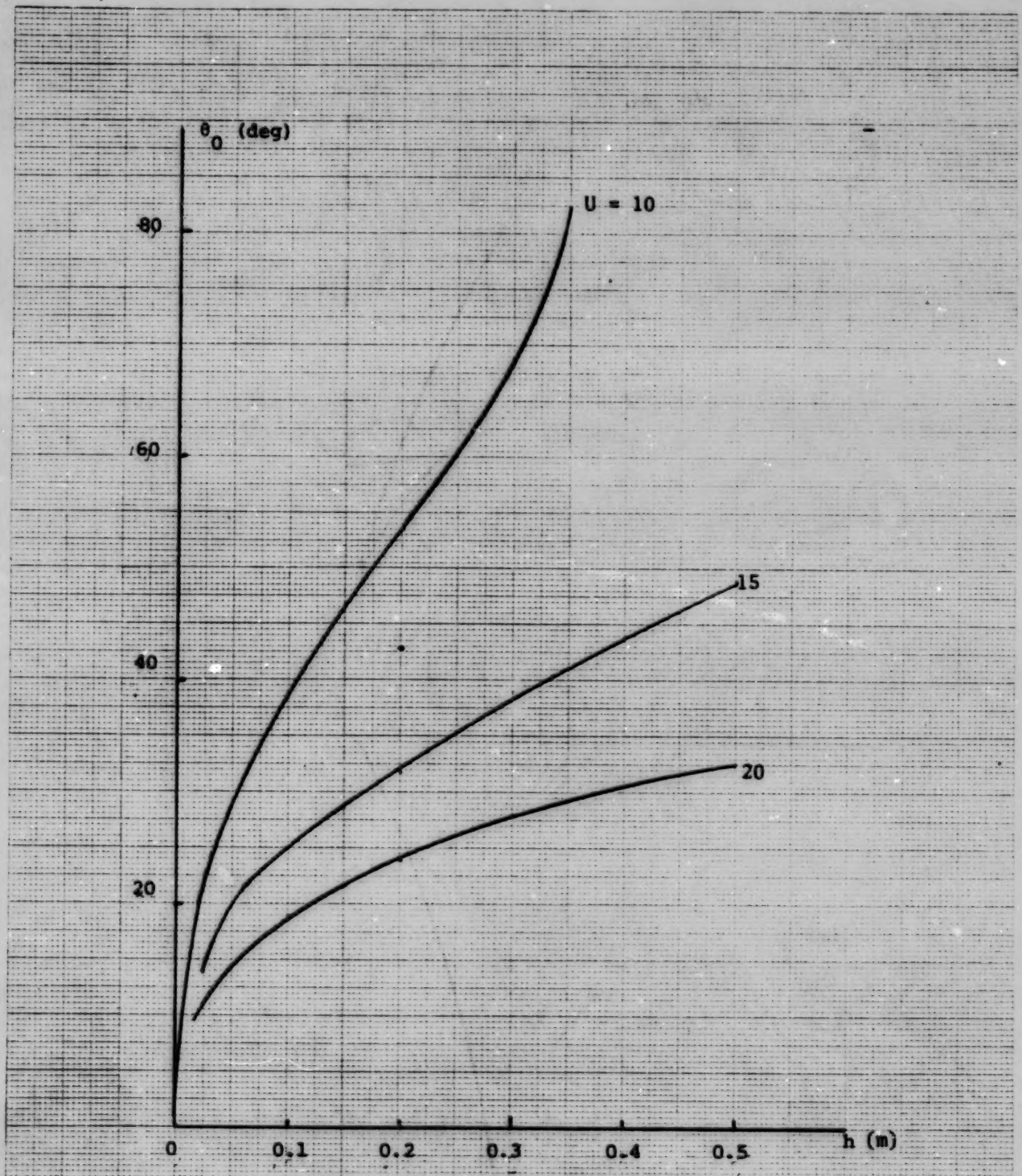

Figure 11. Angle of Radial Crests vs h.

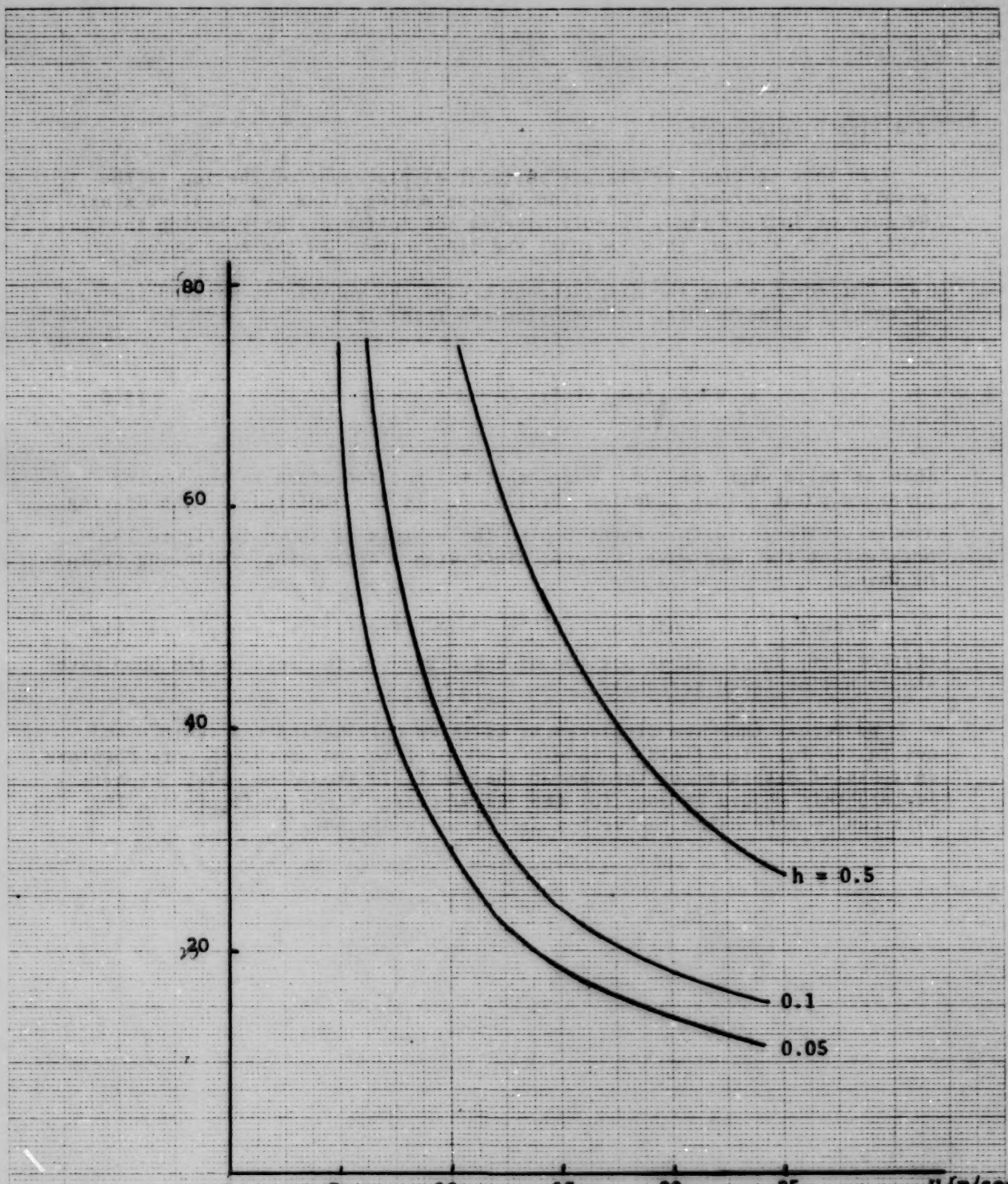

Figure 12. Angle of Radius Crests vs. U.

3.4 Ice Displacement.

In this section, we discuss vertical displacement of the ice as the result of the uniform motion of an impulse moving along the negative x-axis. Because of lack of time, we only discuss the motion directly behing the vehicle. Of course, this includes the displacement in the hump wave.

The formula for the displacement behind the vehicle is derived in appendix F. The result, in dimensionless form, is

$$\eta_S = \frac{P_0}{3}\sqrt{\frac{6}{5\pi\tilde{x}}}\,\sin\left(\tilde{x} - \frac{\pi}{4}\right) \tag{3.3}$$

This is valid when $\varepsilon F^{1/3} r >> \mu h$, that is, not too close to the moving pressure point. (See equation (F13).) P_0 is the amplitude of the driving impulse. The ice displacement behind the vehicle is shown in figure 13. Notice that the hump wave appears, along with a decreasing, following train of waves.

Because of the condition $\varepsilon F^{1/3} r >> \mu h$, the figure is approximately correct for $\tilde{x} > 1$. That portion of the figure to the left of the hump wave should not be taken seriously.

We repeat that ice displacement is shown only behind the vehicle and not in the full ice field because of lack of time and money. A more complete analysis of displacement throughout the ice field should be made; in particular, this should be done for the radial crests shown in figure 4 - 10. This can be done using the method discussed in appendix F.

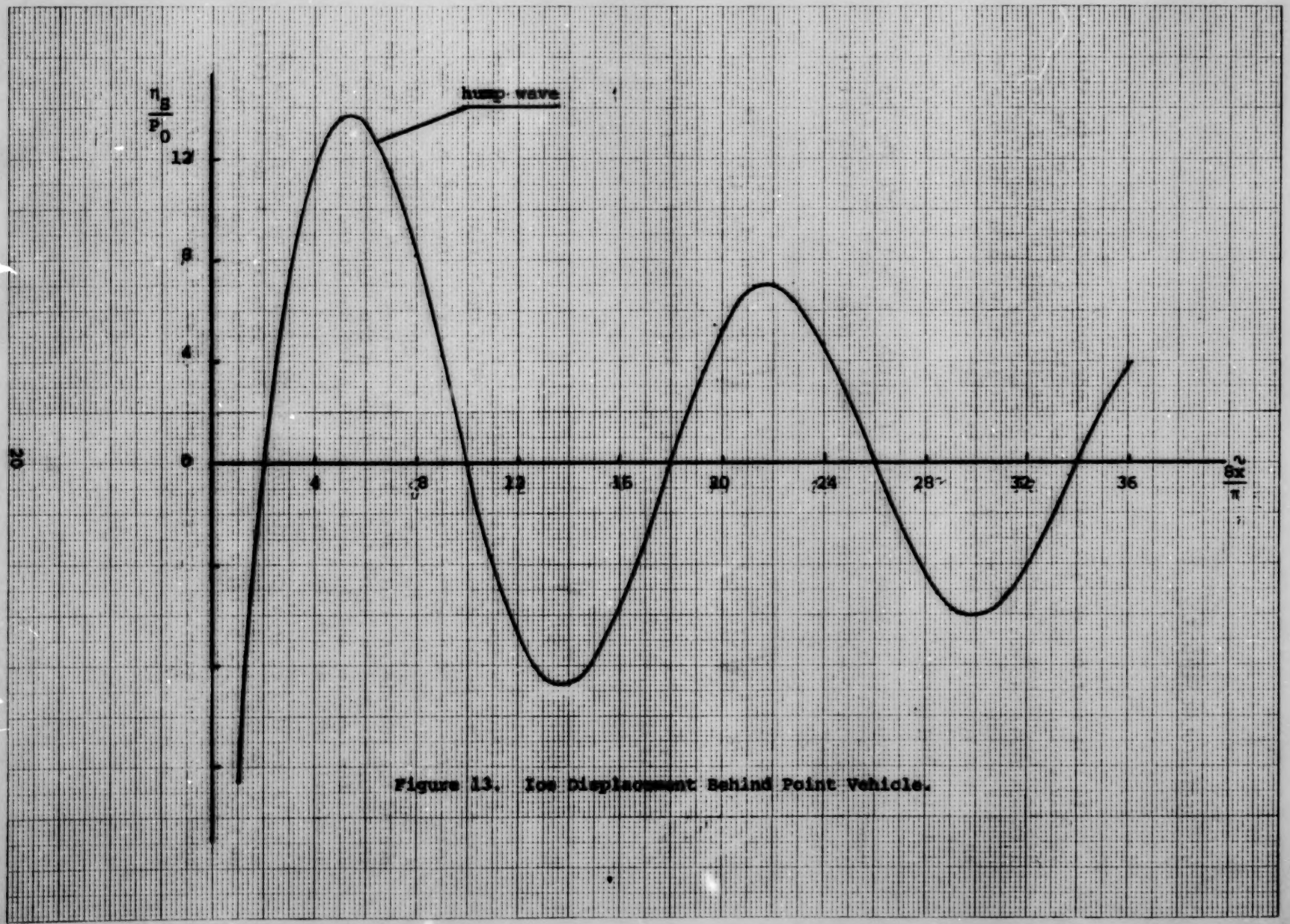

Figure 13. Ice Displacement Behind Point Vehicle.

4. RECTANGULAR VEHICLE.

In this section, we show that our methods apply also to more realistic vehicle configurations than points. Also, we begin an analysis of the question of optimum vehicle aspect ratio for the purpose of breaking ice. Although there has not been enough time for anything like a complete study of this question, it is shown that it may at least be feasible to design an optimum vehicle, and the first step is taken.

4.1 Ice Displacement.

We consider a rectangular vehicle of length $2a$ and width $2b$. We denote the vehicle's area by $A = 4ab$ and its aspect ratio by $\alpha = a/b$. It is shown in appendix G that the displacement directly behind the vehicle has the form

$$\eta_R = \beta_+\sqrt{\frac{2\pi}{\gamma|f_+''|}}\sin\left(\gamma f_+ - \frac{\pi}{4}\right) - \beta_-\sqrt{\frac{2\pi}{\gamma|f_-''|}}\sin\left(\gamma f_- - \frac{\pi}{4}\right), \qquad (4.1)$$

approximately. The quantities occurring here are all defined in appendix G. What is most important to recall is that

$$\gamma = \frac{\varepsilon F^{1/3}}{2\mu h}\sqrt{\frac{A}{\alpha}}\,. \qquad (4.2)$$

Everything in equation (4.1) depends on h and U. Also, γ depends on A and α. Since we are mainly interested in the variation of η_R with α, for the purposes of illustration, we fix the values of h, U and A here at $h = 0.15$ m, $U = 15$ m/sec, and $A = 200$ m^2. The displacement behind the vehicle was calculated for several values of α, using (4.1), and the result plotted in Figure 14. All graphs in the Figure begin directly behind the vehicle, and the depression in the ice due to the vehicle can be clearly seen, as can the hump wave.

It can also be seen that the curves in Figure 14 do not damp out as we move to the right, away from the vehicle. This is because, in deriving (4.1), we have taken γ to be large and have assumed x/a not too large. This was done because interest is focussed on the hump wave. However, it has a consequence that accuracy in Figure 14 decreases as we move to the right.

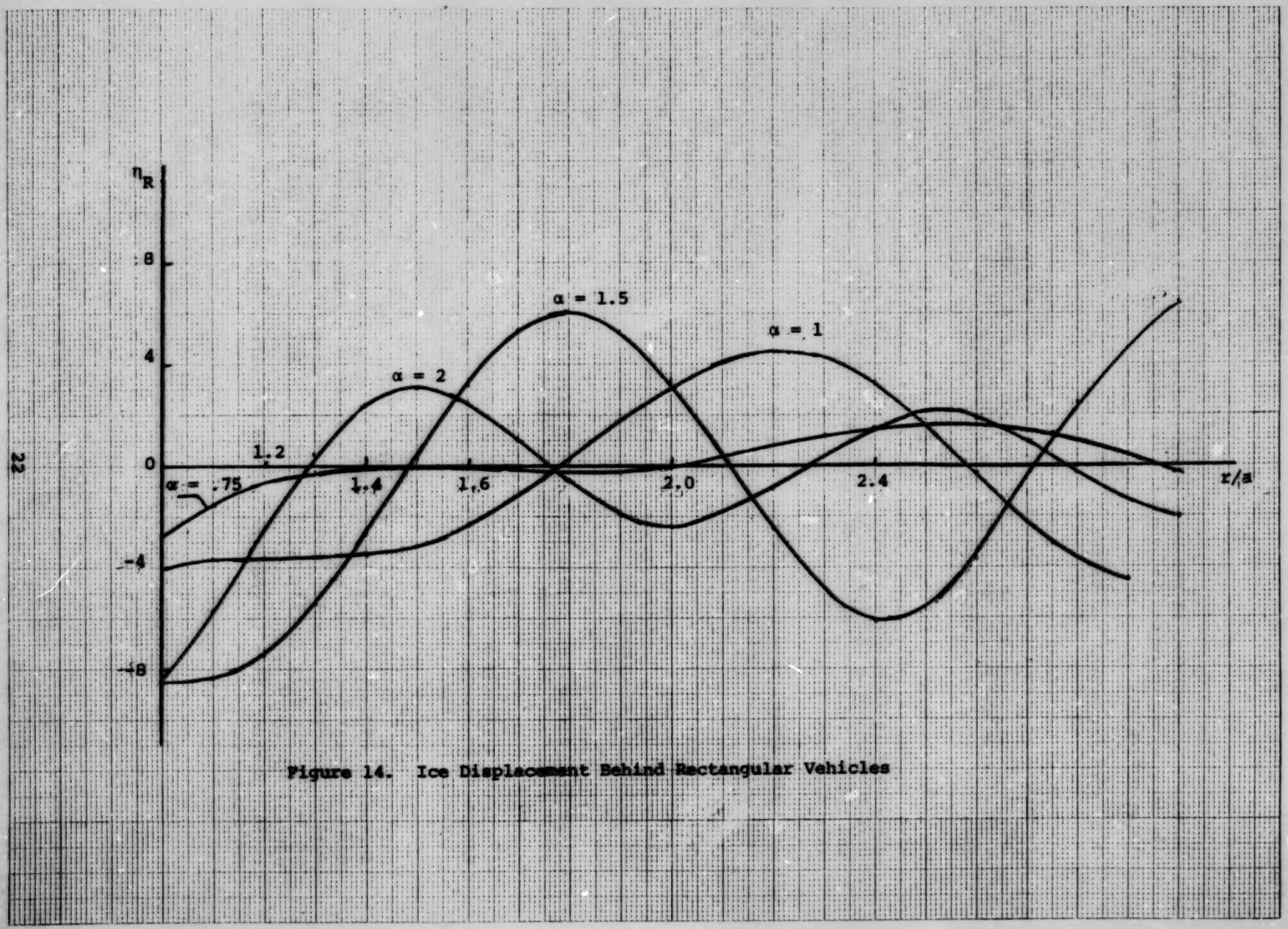

Figure 14. Ice Displacement Behind Rectangular Vehicles

It would be possible, if one were interested in improving the results past the hump wave, to repeat the analysis of appendix G using x/α as the large parameter.

4.2 Stresses Behind the Vehicle.

As we have said several times, the ultimate purpose of this study is to provide a framework within which an optimum vehicle for icebreaking can be designed. Although this has not been possible to achieve because of lack of time and money, we are able to show that such a study is at least feasible using the methods described in this report.

This is done as follows. We consider a rectangular vehicle of given area A and variable aspect ratio α. A is taken to be fixed because it provides a rough measure of the mass of the ACV, and we want to know the effect of changing α for a vehicle of given size. For a given speed U and ice thickness h, the relative stress in the hump wave is considered as a function of α.

Once again, this is a limited thing to do: the stress should be considered in the entire field, in particular, along the radial crests. Also, and most important, the effect of varying h and, particularly, U should be taken into account. However, to show that it is feasible to make progress by this method, we examine the stress in the hump wave at values of h and U chosen at hazard: $h = 0.15$ m, $U = 15$ m/sec, as above. The method for finding the stress (actually, the total force on the ice) is discussed in appendix G.

The result for $A = 200\ m^2$ is shown in Figure 15, from which it is clear that the maximum stress in the hump wave occurs for an aspect ratio about 1.4. For comparison, we note that the ACV Voyageur (which has an area of about $200\ m^2$) has an aspect ratio of about 2. According to Figure 15, then, a vehicle with the same area and mass as the Voyageur, but with aspect ratio reduced from 2 to 1.4 should produce a 37% increase in stress in the hump wave.

It must be repeated again: figure 15 and the number 37% are presented only to show that the method is feasible. Before any of this can be taken seriously in design considerations, it will be necessary to evaluate the effects of varying speed U and ice thickness h. (Also to be considered must be the effect of water depth.) There is no claim here that the value of U used in deriving figure 15 is optimal; it is even possible that the optimal U would produce more than a 37% improvement by changing aspect ratio. However, this is speculative, and a complete answer must be left for future work.

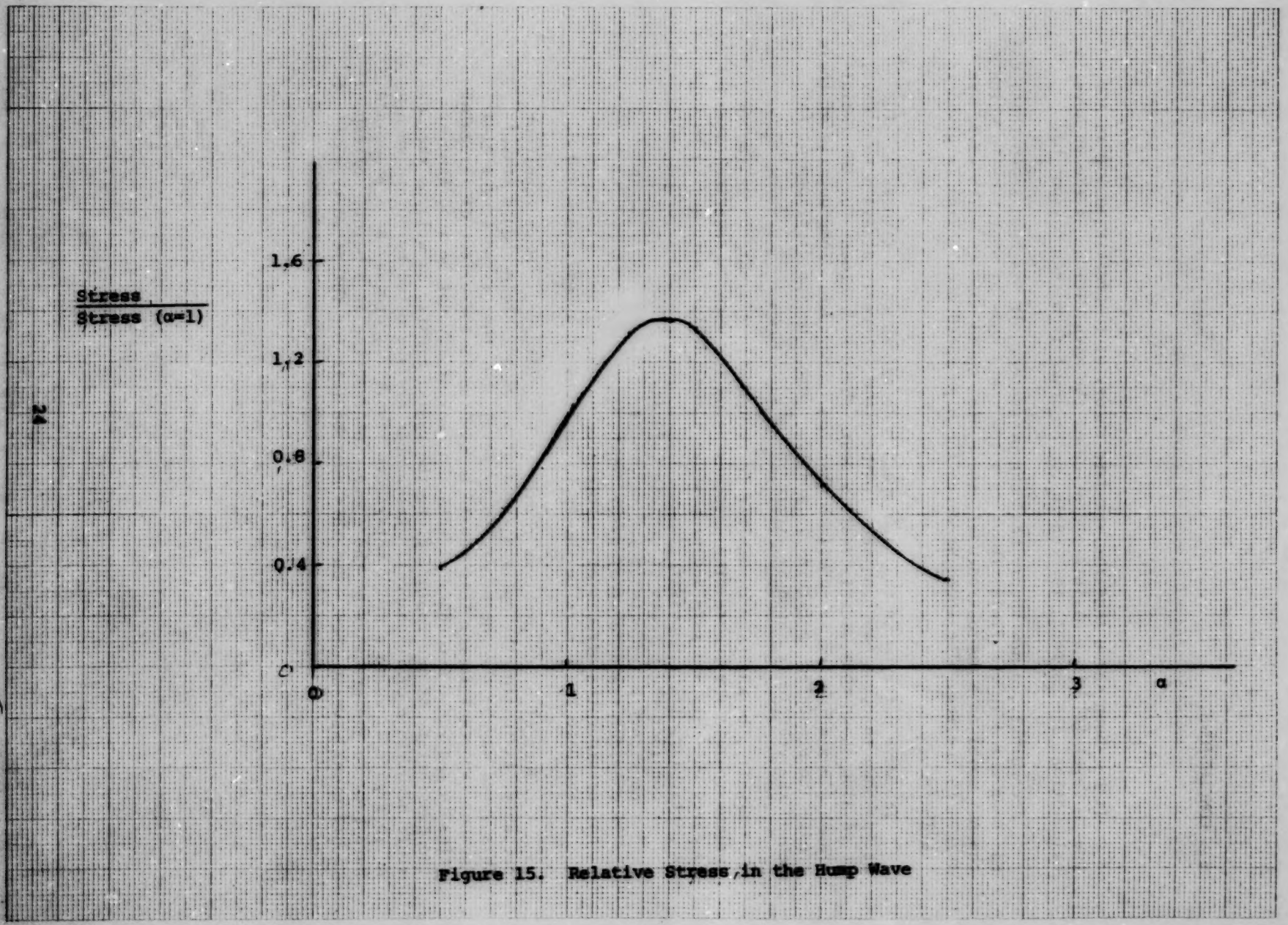

Figure 15. Relative Stress in the Hump Wave

5. CONCLUSIONS

It has been shown that the standard theory of icebreaking using an ACV, due to Nevel [2], is a misinterpretation of the mathematics: although Nevel's calculations are correct, the conclusion he draws from them may not be.

Accordingly, a new theory has been presented. It has been shown that, as has been noted in the field, there is a low speed mode of operation in which the ACV moves in a depression bowl, and a high speed mode in which waves are formed in the ice. The speed at which the high speed mode begins is given in figure 2.

The wave patterns in the high speed mode are shown in figures 4 - 10. It is shown that, as has been seen in the field, there is always a hump wave. It is also shown that radial crests appear; these may account for the radial cracks along which ice is sometimes observed to rupture. Some details of these crests are presented in figures 11 and 12. Next, the ice displacement far behind the vehicle is shown in figure 13.

Finally, it has been shown that it is probably feasible to design an optimum vehicle for icebreaking purposes using the methods described herein. To carry out this analysis and propose an actual design, more has to be done. In particular, it is necessary to

- consider the effects of vehicle velocity,
- consider the effects of ice thickness,
- consider the effects of water depth,
- consider the effects of vehicle area and mass,
- evaluate the errors in the approximations of appendices F and G.

A number of other problems remain to be considered. Most important, probably, is to find the optimum speed at which a vehicle should travel. This speed may be the one predicted by Nevel, but that is no longer clear. Another important factor that should be studied is the effect of irregularities in the ice. Secondary effects that may or may not be important are the possibility of ice rupture along the radial crests, as well as the possible occurrence of resonances. Resonances are suggested by points such as A in figure 4, where a crest intersects itself. There may be a resonance here bacause the branches of the curve, intersecting at a point, correspond to different wave numbers. But this must be left for future work.

6. REFERENCES

1. H. Cohen and A. Clayton, Research into transport aspects of ice sheets. Office of Industrial Research, University of Manitoba. June, 1982.

2. Donald E. Nevel, Moving loads on a floating ice sheet. C.R.R.E.L., Hanover, N.H., U.S.A. May, 1970.

3. Marvin Shinbrot, A preliminary analysis of dynamic ice rupture by hovercraft. Centre de Recherche de Mathématiques Appliquées Report No. 914. Université de Montréal. Transport Canada Report TP2461. January, 1980.

4. Sir Horace Lamb, Hydrodynamics. Cambridge University Press, 1932.

5. J.J. Stoker, Water Waves. Interscience Publishers, Inc. New York, 1957.

6. G.B. Whitham, Linear and Nonlinear Waves. John Wiley & Sons, New York, 1974.

7. M.J. Lighthill, River waves. Naval hydrodynamics publication 515. National Academy of Sciences.- National Research Council (U.S.A.). 1957.

APPENDIX A. The Dispersion Relation

It is well known (see, e.g. [6]) that in any problem involving waves the dispersion relation is fundamental. Accordingly, we derive the relation here.

The equations of a thin plate, supported below by water and supporting a pressure distribution $P(t,x,z)$ are as follows. Taking the depth of the water to be infinite, there is a velocity potential ϕ satisfying

$$\phi_{xx} + \phi_{yy} + \phi_{zz} = 0, \quad y < 0 \tag{A1}$$

with the boundary conditions

$$\phi_y \to 0 \quad \text{as} \quad y \to -\infty \tag{A2}$$

and

$$\phi_y = \eta_t \quad \text{when} \quad y = 0. \tag{A3}$$

Also, Bernoulli's equation gives

$$g\eta + \frac{1}{\rho}p + \phi_t = 0. \tag{A4}$$

The equation for the vertical displacement of the ice is then

$$D\left(\frac{\partial^2}{\partial x^2} + \frac{\partial^2}{\partial z^2}\right)^2 \eta - p + \rho' h \eta_{tt} = -P. \tag{A5}$$

To find the dispersion relation, we take $P = 0$, and we look for a solution in the form

$$\phi = ae^{yk} \cos(\underline{k}\cdot\underline{x} - \omega t),$$

which always satisfies (A1) and (A2). η_t can be calculated from (A3), and then integration with respect to t gives

$$\eta = -\frac{ak}{\omega} \sin(\underline{k}\cdot\underline{x} - \omega t).$$

Then, we get, from (A4),

$$\frac{1}{\rho}p = a\left(\frac{gk}{\omega} - \omega\right) \sin(\underline{k}\cdot\underline{x} - \omega t).$$

Thus, when $P = 0$, we have a solution of (A1) - (A5) when

$$-\frac{Dk^5}{\omega} - \frac{\rho g k}{\omega} + \rho\omega + \rho' hk\omega = 0,$$

or

$$\omega(k) = \sqrt{\frac{k(\rho g + Dk^4)}{\rho + \rho' hk}} \tag{A6}$$

This is the dispersion relation for the problem. Notice that, when $h = 0$, (A6) reduces to $\omega(k) = \sqrt{gk}$, which is the well-known dispersion relation for waves in water, as it should do.

Setting $\kappa = \mu kh/\varepsilon$, we obtain the dispersion relation in terms of dimensionless variables:

$$\omega(k) = \sqrt{\frac{g\varepsilon\kappa}{\mu h} \cdot \frac{1+\kappa^4}{1+\varepsilon\kappa}} = \sqrt{\frac{g\varepsilon}{\mu h}}\, \omega_0(\kappa). \tag{A7}$$

For later use, we also calculate the wave velocity

$$c(k) = \frac{\omega(k)}{k} = \sqrt{\frac{\mu g h}{\varepsilon\kappa} \cdot \frac{1+\kappa^4}{1+\varepsilon\kappa}} = \sqrt{\frac{\mu g h}{\varepsilon}}\, c_0(\kappa), \tag{A8}$$

and the group velocity

$$\begin{aligned} C(k) &= \frac{d}{dk}\omega(k) \\ &= R(k)c(k), \end{aligned} \tag{A9}$$

where

$$R(k) = \frac{1+\kappa^4(5+4\varepsilon\kappa)}{2(1+\kappa^4)(1+\varepsilon\kappa)}. \tag{A10}$$

APPENDIX B. Nevel's solution

To solve (A1) - (A5), Nevel assumes the ACV moves with constant speed along the negative x-axis with constant speed U. Replacing x by x - Ut amounts to looking at the problem in a coordinate system fixed in the vehicle. In the steady situation, then, ϕ and η no longer depend on t (in the new coordinates) and (A1) - (A5) become

$$\phi_{xx} + \phi_{yy} + \phi_{zz} = 0, \quad y < 0, \tag{B1}$$

$$\phi_y \to 0 \quad \text{as} \quad y \to -\infty, \tag{B2}$$

$$\phi_y - U\eta_x = 0 \quad \text{when} \quad y = 0, \tag{B3}$$

$$g\eta + \frac{1}{\rho}p + U\phi_x = 0 \quad \text{when} \quad y = 0, \tag{B4}$$

$$D\left(\frac{\partial^2}{\partial x^2} + \frac{\partial^2}{\partial z^2}\right)^2 \eta - p + \rho' h U^2 \eta_{xx} = -P. \tag{B5}$$

To solve these equations, take the Fourier transform of (B1). This gives

$$\hat{\phi}_{yy} - k^2\hat{\phi} = 0. \tag{B6}$$

In view of (B2), the solution of (B6) that we want has the form of a function of $\underline{k}$ alone times e^{yk}. Using (B3), then, we find

$$\hat{\phi} = -\left[\frac{iUk_1}{k}\hat{\eta}\right]e^{yk}.$$

Substituting this into the Fourier transform of (B4) we find, after some simplification,

$$\hat{p} = \rho\left(\frac{U^2k_1^2}{k} - g\right)\hat{\eta}.$$

Finally, then, the Fourier transform of (B5) gives

$$\hat{\eta} = \frac{\hat{p}}{\rho} \cdot \frac{k}{(1+\mu hk)(U^2k_1^2-\omega^2)}, \tag{B7}$$

where $\omega = \omega(k)$ is the dispersion relation, defined by (A6).

Taking the inverse Fourier transform of (B7), we find, along with Nevel, that the ice displacement at the origin is given by

$$\eta(0,0) = \frac{1}{(2\pi)^2}\int_{-\infty}^{\infty}\int_{-\infty}^{\infty} \frac{\hat{p}(k_1,k_2)}{\rho} \cdot \frac{k}{(1+\mu hk)(U^2k_1^2-\omega^2)}\, dk_1\, dk_2$$

$$= \frac{1}{(2\pi)^2}\int_0^{\infty}\int_0^{2\pi} \frac{k^2\hat{p}(k)d\psi\, dk}{\rho(1+\mu hk)(U^2k_1^2\cos^2\psi - \omega^2)},$$

in polar coordinates. Here, we have assumed the vehicle to be circularly symmetric, so that p is a function only of the distance from the origin; in that case, $\hat{p}$ depends only on k. The integral with respect to ψ is elementary and can be evaluated. The result then is

$$\eta(0,0) = \frac{1}{4\pi}\int_0^{\infty} \frac{k^2\hat{p}(k)dk}{(1+\mu hk)\omega\sqrt{\omega^2-\rho U^2k}}. \tag{B8}$$

Now, the demonimator here is zero when $\omega^2 = \rho U^2 k$. When this zero is a <u>double</u> zero, the integral is infinite. Thus, $\eta(0,0)$ is infinite when

$$\left.\begin{aligned} \omega^2(k) &= \rho U^2 k \\ 2\omega(k)C(k) &= \rho U^2, \end{aligned}\right\} \tag{B9}$$

where $C(k)$ is the group velocity. (See (A9).)

Equations (B9) are two equations for k and U. The value of U that one finds by solving (B9) is Nevel's critical velocity v_{crit}. At this velocity, the integral (B8) diverges, and $\eta(0,0)$ is infinite.

Notice that the only parameters appearing in (B8) are ρ, ρ', h, and D. Thus, v_{crit} can only depend on these parameters, so that v_{crit} does not depend on anything to do with the vehicle. This is the source of the running mouse paradox.

APPENDIX C. The Impulse Response

In this appendix, we find the exact solution to equations (A1) - (A5) when the applied pressure P is a single impulse applied at the origin at time zero. Thus we take

$$P = \delta(x)\delta(z)\delta(t). \tag{C1}$$

(A1) - (A5) are again solved using Fourier transforms.

As in appendix B, (A1) - (A2) give that $\hat{\phi}$ is e^{yk} times a function that does not depend on y. (A3) then gives

$$\hat{\phi} = \frac{e^{yk}}{k} \cdot \frac{\partial \hat{\eta}_0}{\partial t} \tag{C2}$$

and (A4) given

$$-\frac{1}{\rho}\hat{p} = g\hat{\eta}_0 + \frac{1}{k}\frac{\partial^2 \hat{\eta}_0}{\partial t^2} \tag{C3}$$

Because of (C1), $\hat{p} = \delta(t)$. Substituting this, (C2), and (C3) in (A5), we find, after some manipulation,

$$\frac{\partial^2 \hat{\eta}_0}{\partial t^2} + \omega^2(k)\hat{\eta}_0 = -\frac{k\delta(t)}{\rho+\rho' hk} \tag{C4}$$

(C4) is an ordinary differential equation that is easily solved. Assuming the ice is quiescent before the impulse strikes, $\hat{\eta} = 0$ for $t < 0$ and then (C4) gives

$$\hat{\eta}_0 = -\frac{k}{\rho+\rho' hk} \cdot \frac{\sin \omega t}{\omega}, \quad t > 0. \tag{C5}$$

APPENDIX D. The Response to a Moving Impulse

Here, we find the transient response of the ice to an impulse starting at the origin and moving with constant speed U along the negative x-axis. This response can be looked upon as the result of an infinite number of infinitesimal impulses striking the ice at successive points on the x-axis. Thus, we consider first the result of infinitesimal impulses applied at times $0, t_0, 2t_0, \ldots$ at the points $0, -Ut_0, -2Ut_0, \ldots$ of the x-axis. For $t < t_0$, the response is just the impulse response of appendix C:

$$\eta(t,x,z) = t_0\eta_0(t,x,z), \quad 0 \le t < t_0 .$$

In the next interval of time, the responses add, so that

$$\eta(t,x,z) = t_0[\eta_0(t,x,z) + \eta_0(t-t_0,x+Ut_0,z], \quad t_0 \le t < 2t_0 .$$

In general, after $k+1$ pulses have occurred,

$$\eta(t,x,z) = t_0 \sum_{j=0}^{k} \eta_0(t-jt_0,x+jUt_0,z), \quad kt_0 \le t < (k+1)t_0 .$$

Letting t_0 go to zero in this formula, we find

$$\eta(t,x,z) = \int_0^t \eta_0(t-t',x+Ut',z)dt'$$

$$= \int_0^t \eta_0(t',x+Ut-Ut',z)dt'.$$

This is the desired response. However, it is more convenient to consider it in a coordinate system moving with the impulse. Thus, we replace $x + Ut$ by x to find

$$\eta(t,x,z) = \int_0^t \eta_0(t',x-Ut',z)dt'. \qquad \text{(D1)}$$

We remind the reader that η_0 is the function whose Fourier transform is given in (C5).

To be able to compare our results with Nevel's, we take the Fourier transform of (D1). The result is

$$\hat{\eta}(t,\underline{k}) = \int_{-\infty}^{\infty}\int_{-\infty}^{\infty} e^{i\underline{k}\cdot\underline{x}} \int_0^t \eta_0(t',x-Ut',z)dt'\,dx\,dz$$

$$= \int_0^t e^{iUk_1t'}\,\hat{\eta}_0(t',\underline{k})dt'$$

$$= -\int_0^t e^{iUk_1t'}\,\frac{k}{\rho+\rho' hk}\cdot\frac{\sin\,\omega t'}{\omega}\,dt' \ ,$$

by (C5). Now, this integral is elementary, and we can evaluate it to find

$$\hat{\eta}(t,\underline{k}) = \frac{k}{2(\rho+\rho' hk)\omega(k)}\left[\frac{1-e^{it(Uk_1-\omega(k))}}{Uk_1-\omega(k)} - \frac{1-e^{it(Uk_1+\omega(k))}}{Uk_1+\omega(k)}\right]. \qquad (D2)$$

This is the Fourier transform of the response to an impulse beginnint at $t = 0$ and moving with speed U in the direction of the negative x-axis.

APPENDIX E. Equations for the Wave Pattern

To derive the wave patterns, we follow the analysis in Whitham [6, chap. 12], where the work is done very efficiently. We treat the vehicle as a moving pressure point and introduce a coordinate system moving with the point. In this moving coordinate system the dispersion relation is $Uk_1 + \omega(k) = k[-U \cos \psi + c(k)]$, and this is zero if the wave appear steady when viewed from the vehicle. (See equation (2.1).) Thus, we have

$$Uk_1 + \omega(k) = 0 . \tag{E1}$$

We want to describe the wave pattern. To do so, we concentrate on a fixed phase of the patterns, say, the crests. Only certain wave numbers contribute to forming the crests, and these wave numbers depend, naturally, on x and z. Now, given any phase θ describing a steady wave pattern, the definition of the wave numbers k_1 and k_2 is

$$k_1 = \frac{\partial \theta}{\partial x} , \quad k_2 = \frac{\partial \theta}{\partial z} .$$

It follows immediately from this equation that

$$\frac{\partial k_1}{\partial z} = \frac{\partial k_2}{\partial x} . \tag{E2}$$

(See [6, eq. (11.43)].)

From (E1), $\omega(k_1,k_2) = Uk_1 + \omega(k) = 0$, so that

$$\frac{\partial \omega}{\partial k_1} \cdot \frac{\partial k_1}{\partial z} + \frac{\partial \omega}{\partial k_2} \cdot \frac{\partial k_2}{\partial z} = 0 ,$$

and, from (E2),

$$\frac{\partial \omega}{\partial k_1} \frac{\partial k_2}{\partial x} + \frac{\partial \omega}{\partial k_2} \frac{\partial k_2}{\partial z} = 0 .$$

This shows that k_2 is constant on the curves satisfying

$$\frac{\partial z}{\partial x} = \frac{\partial\omega/\partial k_2}{\partial\omega/\partial k_1}$$

$$= \frac{k_2 C(k)}{Uk + k_1 C(k)}$$

$$= \frac{C(k)\tan\psi}{c(k)\sec^2\psi - C(k)} .$$

Thus, if (r,χ) are polar coordinates in the (x,z) plane, we have

$$\tan\chi = \frac{C(k)\tan\psi}{c(k)\sec^2\psi - C(k)} . \tag{E3}$$

To find parametric equations for the wave crests, it remains to find an equation for r. Now, again if θ is any phase of the pattern,

$$\theta = \int_0^{\underline{x}} \underline{k} \cdot d\underline{x} . \tag{E4}$$

Because of (E2), we may integrate along any path connecting the origin to $\underline{x}$, and we choose the straight line segment. This gives $d\underline{x} = (\cos\chi, \sin\chi)dr$, while, of course $\underline{k} = (-k\cos\psi, k\sin\psi)$. Thus, $\underline{k} \cdot d\underline{x} = -k\cos(\chi+\psi)dr$, so that by (E4), $\theta = -kr\cos(\chi+\psi)$. Thus,

$$r = -\frac{\theta}{k\cos(\chi+\psi)}$$

$$= -\frac{\theta}{k}\frac{\sqrt{U^2 + C^2 - 2UC\cos\psi}}{C - c} ,$$

where (E3) has been used. Using this formula and (E3) in $x = r\cos\chi$, $x = r\sin\psi$, we find

$$\left.\begin{aligned} x &= -\theta \cdot \frac{U - C\cos\psi}{k(C-c)} \\ z &= -\theta \cdot \frac{C\sin\psi}{k(C-c)} \end{aligned}\right\} \tag{E5}$$

Now, we use (2.1). This gives

$$\left.\begin{aligned} x &= \frac{\theta}{U} \cdot \frac{U^2 - C(k)c(k)}{k[c(k) - C(k)]} \\ z &= \frac{\theta}{U} \cdot \frac{C(k)\sqrt{U^2 - c^2(k)}}{k[c(k) - C(k)]} \end{aligned}\right\} \qquad \text{(E6)}$$

These are the parametric equations for the curves at a given phase θ. $k \geq 0$ is the parameter.

It is convenient to write (E6) in dimensionless form, by taking $k = \varepsilon\kappa/\mu h$. Also, we recall $C = Rc$. With these substitutions, (E6) becomes

$$\left.\begin{aligned} \xi &= \theta \cdot \frac{F - Rc_0^2}{\kappa\, c_0(1-R)} \\ \zeta &= \theta \cdot \frac{R\sqrt{F - c_0^2}}{\kappa(1-R)} \end{aligned}\right\} \qquad \text{(E7)}$$

This is the final form of the parametric equations. θ is the phase and is fixed for any curve. κ is the parameter, and

$$c_0(\kappa) = \sqrt{\frac{1 + \kappa^4}{\kappa(1+\varepsilon\kappa)}}\,.$$

As a check on our results, we consider the case $h = 0$. One cannot conveniently let h go to zero in (E7), as the limit is singular. Therefore, we return to (E5), from which equations (E7) were derived When $h = 0$, $C = \frac{1}{2}c$, and $R = \frac{1}{2}$. Also, as we remarked in Appendix A, when $h = 0$, $\omega_0 = \sqrt{gk}$, so that $c = \sqrt{g/k}$. Substituting these limits into (E5), and using the fact that $U \cos\psi = c(k)$ to eliminate k, we find

$$\left.\begin{aligned} x &= -\frac{\theta U^2}{g}\cos\psi(1 + \sin^2\psi) \\ z &= -\frac{\theta U^2}{g}\sin\psi\cos^2\psi \end{aligned}\right\} \qquad \text{(E8)}$$

for the equations of the curves of constant phase when $h = 0$. Here, ψ is the parameter. Equations (E8) are the standard equations, first derived by Kelvin in 1887, for the wave pattern produced on water of infinite depth by a moving pressure point. (See, e.g., [6, (12.36)].)

APPENDIX F. Steady Ice Displacement Due to a Moving Impulse

The Fourier transform of the transient ice displacement due to a moving impulse is given by equation (D2) and, as we pointed out, it is not permissible to let t go to infinity in this formula. To find the ice displacement in steady motion then, we resort to an artifice due to Lighthill [7]. In equations (A1) - (A5), we replace the driving pressure P by a function of the form $e^{\delta t}P$, where $\delta > 0$. This amounts to a pressure that was essentially zero in the distant past which gradually grew until, at current times, it is close to the actual pressure. At the end, we let δ tend to zero.

Thus, in (A1) - (A5), we replace P by $e^{\delta t}P$; also, we suppose that the new P depends only on $x + Ut$ and z. Replacing ϕ and η by $e^{\delta t}\phi$ and $e^{\delta t}\eta$ and looking at the problem in a coordinate system moving with the pressure point, then, we find that (A1) - (A5) become

$$\phi_{xx} + \phi_{yy} + \phi_{zz} = 0, \quad y < 0 , \tag{F1}$$

$$\phi_y \to 0 \quad \text{as} \quad y \to -\infty , \tag{F2}$$

$$\phi_y = \delta\eta + U\eta_x, \quad y = 0 , \tag{F3}$$

$$g\eta + \frac{1}{\rho} p + \delta\phi + U\phi_x = 0, \quad y = 0 \tag{F4}$$

$$D\left(\frac{\partial^2}{\partial x^2} + \frac{\partial^2}{\partial z^2}\right)^2 \eta - p + \rho' h(\delta^2\eta + 2\delta U^2\eta_{xx} + U^2\eta_{xx}) = -P, \quad y = 0 . \tag{F5}$$

Taking Fourier transforms (which is now legitimate - as we shall see - because of the factor $e^{\delta t}$), we can solve (F1) - (F5) as we solved (B1) - (B5) in appendix B. The result is

$$\hat{\eta}(\underline{k}) = \frac{1}{\rho} \cdot \frac{k\,\hat{P}(k)}{1 + \mu hk} \cdot \frac{1}{(Uk_1 + i\delta)^2 - \omega^2(k)} . \tag{F6}$$

Notice that this would be the same as Nevel's formula (B7) were we to set $\delta = 0$. However, (F6) is never infinite because δ is <u>not</u> zero.

Using the formula for the inverse Fourier transform, and writing $k = \varepsilon\kappa/\mu h$ in that formula, we find, after some simplification,

$$\eta(x,z) = \frac{1}{4\pi^2\rho g}\int_{-\infty}^{\infty}\int_{-\infty}^{\infty}\frac{\kappa\,\hat{\beta}(\underline{\kappa})e^{-\frac{i\varepsilon}{\mu h}(\underline{\kappa}\cdot\underline{x})}}{1+\varepsilon\kappa}\cdot\frac{d\kappa_1\,d\kappa_2}{F(\kappa_1+i\delta)^2-\omega_0^2(\kappa)}$$

Now, let $x = r\cos\chi$, $z = r\sin\chi$, $\kappa_1 = -\kappa\cos\psi$, $\kappa_2 = \kappa\sin\psi$. In these coordinates, we find

$$\eta = \frac{1}{4\pi^2\rho g}\int_{-\pi}^{\pi}\int_{0}^{\infty}\frac{\kappa^2\,\hat{\beta}\,e^{\frac{i\varepsilon}{\mu h}\kappa\, r\cos(\psi+\chi)}}{1+\varepsilon\kappa}\cdot\frac{d\kappa\,d\psi}{F(\kappa\cos\psi-i\delta)^2-\omega_0^2(\kappa)}\,.$$

The integral from $-\pi$ to $-\pi/2$ is the conjugate of the integral from 0 to $\pi/2$, and the integral from $\pi/2$ to π is the conjugate of the integral from $\pi/2$ to π. Thus, we may replace the integral from $-\pi$ to π by the real part of the integral from $-\pi/2$ to $\pi/2$. Also, we must let δ go to zero. Thus, we obtain, finally,

$$\eta = \frac{1}{2\pi^2\rho g}\lim_{\delta\to 0}\operatorname{Re}\int_{-\pi/2}^{\pi/2}\int_{0}^{\infty}\frac{\kappa^2\,\hat{\beta}\,e^{\frac{i\varepsilon}{\mu h}\kappa\, r\cos(\psi+\chi)}}{1+\varepsilon\kappa}\cdot\frac{d\kappa\,d\psi}{F(\kappa\cos\psi-i\delta)^2-\omega_0^2(\kappa)} \qquad \text{(F7)}$$

It is our purpose here to evaluate this integral when P is an impulse and $\chi = 0$ (in the hump wave). We do this by evaluating the inner integral asumptotically by residues. For this, we examine the roots of the denominator of (F7), that is, the solutions of

$$\kappa(1+\kappa^4) = \lambda^3(\kappa+i\delta_1)^2(1+\varepsilon\kappa), \qquad \text{(F8)}$$

where $\delta_1 = \delta/\cos\psi$. We shall see that the points where $\cos\psi = 0$ ($\psi = \pm\pi/2$) do not contribute sensibly to the integral, so that δ_1 goes to zero when δ does.

Now, (F8) has five solutions. Two of them are small for λ large and δ small; these poles do not contribute much to (F7) because of the term

κ^2 in the numerator. Two other solutions of (F8) have complex limits and are $0(\lambda)$ as $\delta \to 0$. These give exponentially small contributions to the integral when the path of integration is rotated to the positive imaginary κ-axis. Thus, upon rotation of the path of integration to the positive imaginary axis in the κ-plane, the only pole that contributes sensibly is the nearly real solution of (F8).

In (F8), set $\kappa = \lambda K$ and $\delta = 0$. Then, if $K \neq 0$, we find

$$\frac{1}{\lambda^4} + K^4 = K(1+\varepsilon\lambda K).$$

It follows that $K = K_0 + 0(1/\lambda^4)$ as $\lambda \to \infty$, where K_0 satisfies

$$K_0^3 = 1 + \varepsilon\lambda K_0 \qquad \text{(F9)}$$

Now, a simple calculation shows that when $E = 3 \times 10^9$Pa, $\sigma = 1/3$, $\rho = 10^3$ kg/m^3, $\mu = 0.9$, and $g = 9.8$ m/sec., we have

$$\varepsilon = .0690h^{1/4} \quad \text{and} \quad F = .00782\,\frac{U^2}{h^{3/4}}.$$

Thus,

$$\lambda = .1985\,\frac{U^{2/3}}{h^{1/4}}\cos^{2/3}\chi \leq .1985\,\frac{U^{2/3}}{h^{1/4}},$$

so that $\varepsilon\lambda \leq .0137\,U^{2/3}$. If we suppose for convenience that $U \leq 20$ m/sec., this gives $\varepsilon\lambda \leq .1009$. Now, (F9) can easily be solved numerically, with the results shown in the following table.

$\varepsilon\lambda$	0	.05	.1	.1009
K_0	1	1.017	1.033	1.034

Thus, approximating K_0 to be 1 involves an error of about 3.4% if $U \leq 20$ m/sec. In what follows, then, we take $K_0 = 1$. This gives $K = 1 + 0(1/\lambda^4)$ and $\kappa = \lambda + 0(1/\lambda^3)$ for the nearly real solution of (F8). The actual solution of (F8) near this one is then

$$\kappa = \lambda + i\kappa_1\delta + 0\left(\frac{1}{\lambda^3} + \delta^2\right) \text{ as } \lambda \to \infty \text{ and } \delta \to 0. \qquad \text{(F10)}$$

Here, $\kappa_1 > 0$.

Now, suppose that P_- is an impulse. Then, $\hat{P} = P_0$, a constant. As we pointed as in the discussion of figure 3, the wave pattern is symmetric about the x-axis, so we may suppose $0 \le \chi \le \pi$. When $\cos(\chi+\psi) < 0$, we rotate the path of integration in the inner integral of (F7) through the lower half-plane to the negative imaginary axis. The poles do not contribute, and the integral along the negative imaginary axis is small. Thus, when $\cos(\chi+\psi) < 0$, η is small.

When $\cos(\chi+\psi) \ge 0$, on the other hand, we rotate the path of integration through the upper half-plane to the positive imaginary axis. Again, the integral part is small, as are the contributions from four of the five poles of the integrand of (F7). The pole (F10) is the only one that contributes substantially, and we find

$$\eta \sim \frac{P_0}{3\pi\rho g F^{2/3}} \int_{-\pi/2}^{\pi/2-\chi} \frac{\sin\left[\frac{\varepsilon r F^{1/3}}{\mu h} \cos^{2/3}\psi \cos(\psi+\chi)\right]}{\cos^{4/3}\psi} d\psi \,. \qquad \text{(F11)}$$

When $\varepsilon r F^{1/3}/\mu h$ is large, we may apply the method of stationary phase to this integral.

This method gives that an integral of the form

$$\int_a^b \beta(\psi) \sin[\gamma f(\psi)] d\psi \sim \sum \beta(\psi_0) \sqrt{\frac{2\pi}{\gamma |f''(\psi_0)|}} \sin\left[\gamma f(\psi_0) \pm \frac{\pi}{4}\right], \ \gamma >> 1 \,. \qquad \text{(F12)}$$

Here, ψ_0 denotes any point where the derivative of f is zero, and the ambiguous sign agrees with that of $f''(\psi_0)$. The sum is over all points where f' is zero. To apply this formula to (F11), let

$$\beta(\psi) = \frac{1}{\cos^{4/3}\psi}, \quad \gamma = \frac{\varepsilon r}{\mu h} F^{1/3},$$

$$f(\psi) = \cos^{2/3}\psi \cos(\psi+\chi)$$

The points of stationary phase are the solutions of

$$3 \tan[\chi+\psi_0(\chi)] + 2 \tan \psi_0(\chi) = 0 \ .$$

This equation can be solved explicitly to find

$$\tan \psi_0(\chi) = \frac{5 \pm \sqrt{25+24 \tan^2 \chi}}{4 \tan \chi} \tag{F13}$$

In the interest of brevity, we look only directly behind the pressure point $(\chi = 0)$. In this case, we find $\psi_0 = 0$ also, and a simple calcution gives $f''(0) < 0$ when $\chi = 0$. Thus, the method of stationary phase results in the formula

$$\eta \sim \frac{P_0}{3\rho g} \sqrt{\frac{6h\mu}{5\pi\varepsilon r F^{2/3}}} \sin\left(\frac{\varepsilon F^{1/3} r}{\mu h} - \frac{\pi}{4}\right) , \tag{F14}$$

valid directly behind the vehicle $(\chi = 0)$ when $\varepsilon F^{1/3} r >> h$.

APPENDIX G. The Rectangular Vehicle

The displacement of the ice due to a pressure distribution P is given by (F7). In this appendix, we consider a rectangular vehicle of length $2a$ and width $2b$. For such a vehicle,

$$\hat{P} = \frac{4P_0}{k_1 k_2} \sin(ak_1)\sin(bk_2)$$

$$= \frac{4\mu^2 h^2 P_0}{\epsilon^2} \cdot \frac{\sin\left(\frac{\epsilon a}{\mu h}\kappa \cos\psi\right)\sin\left(\frac{\epsilon b}{\mu h}\kappa \sin\psi\right)}{\kappa^2 \sin\psi \cos\psi},$$

where P_0 is the cushion pressure, assumed constant. Substituting this formula in (F7) and taking $\chi = 0$, we find

$$\eta = \frac{2\mu^2 h^2 P_0}{\pi^2 \epsilon^2 \rho g} \lim_{\delta \to 0} \mathrm{Re} \int_{-\frac{\pi}{2}}^{\frac{\pi}{2}} \int_0^{\infty} \frac{\sin\left(\frac{\epsilon a}{\mu h}\kappa \cos\psi\right)\sin\left(\frac{\epsilon b}{\mu h}\kappa \sin\psi\right)}{(1+\epsilon\kappa)\sin\psi \cos\psi} \cdot \frac{e^{\frac{i\epsilon}{\mu h}\kappa r \cos\psi}}{\omega_0^2(\kappa) - F(\kappa\cos\psi - i\delta)^2} \cdot d\kappa\, d\psi \quad \text{(G1)}$$

Notice that by taking $\chi = 0$, we are restricting our attention to the ice directly behind the vehicle. This restriction is made here for lack of time.

The integrand in (G1) is an even function of ψ; this allows us to replace the integral by twice the integral over the range $0 \le \psi \le \pi/2$. In (G1), use the formula $\sin z = (e^{iz} - e^{-iz})/2i$. Substituting in (G1) and multiplying out the exponentials, we get a sum of four terms, each involving an exponential of the form

$$e^{\frac{i\epsilon\kappa}{\mu h}(r \cos\psi \pm a \cos\psi \pm b \sin\psi)} .$$

Each of these terms can be written as a sum of two, depending on the sign of $(r \pm a)\cos\psi \pm b \sin\psi$. Whenever the sign is negative, we rotate the path of integration in the κ-plane to the negative imaginary axis. The nearly real pole does not contribute and the integral is the small when λ is large.

When $(r \pm a)\cos\psi \pm b \sin\psi > 0$, on the other hand, we rotate to the positive maginary axis, getting a contribution from the principal pole, as in appendix F. Thus we have a sum of four integrals, the ranges of integration being defined by (recall that $0 \le \psi \le \pi/2$ in all cases)

$$\left.\begin{aligned} &(r+a)\cos\psi + b\sin\psi \ge 0, \text{ or } 0 \le \psi \le \pi/2 , \\ &(r+a)\cos\psi - b\sin\psi \ge 0, \text{ or } 0 \le \tan\psi \le \frac{r+a}{b} , \\ &(r-a)\cos\psi + b\sin\psi \ge 0, \text{ or } 0 \le \psi \le \pi/2 \text{ (since } r \ge a) , \\ &(r-a)\cos\psi - b\sin\psi \ge 0, \text{ or } 0 \le \tan\psi \le \frac{r-a}{b} . \end{aligned}\right\} \quad \text{(G2)}$$

The residue at the principal pole $\kappa = \lambda + 0\left(\frac{1}{\lambda^3}\right)$ is

$$\frac{1}{3\lambda^4(1-\varepsilon\lambda)\sin\psi\cos\psi} ,$$

to lowest order in λ, and omitting the exponentials for now. As in appendix F, we omit the term $\varepsilon\lambda$. Then, we obtain, from (G1) and the preceding discussion, that

$$\frac{\eta_R}{F^{4/3}} = \int_0^{\pi/2} \frac{\sin\left[\frac{\varepsilon\lambda}{\mu b}(r+a)\cos\psi + b\sin\psi\right] - \sin\frac{\varepsilon\lambda}{\mu h}\left[(r-a)\cos\psi + b\sin\psi\right]}{\lambda^4\sin\psi\cos\psi}$$

(G3)

$$- \int_0^{\arctan\frac{r+a}{b}} \frac{\sin\frac{\varepsilon\lambda}{\mu h}[(r+a)\cos\psi - b\sin\psi]}{\lambda^4\sin\psi\cos\psi}\,d\psi + \int_0^{\arctan\frac{r-a}{b}} \frac{\sin\frac{\varepsilon\lambda}{\mu h}[(r-a)\cos\psi - b\sin\psi]}{\lambda^4\sin\psi\cos\psi}\,d\psi ,$$

approximately.

Applying now the method of stationary phase to the last two integrals, we find that they do not contribute substantially to the final result, since the point of stationary phase lies outside the range of integration. This leaves only the first integral in (G3).

Set $\gamma = \varepsilon F^{1/3} b/\mu h$, $\tau_{\pm} = (r \pm a)/b$. In this notation, we find, omitting the last two terms in (G3) and using the definition of λ,

$$\eta_R = \int_0^{\pi/2} \Big\{ \sin[\gamma \cos^{2/3} \psi (\tau_+ \cos \psi + \sin \psi)$$

$$- \sin[\gamma \cos^{2/3} \psi (\tau_- \cos \psi + \sin \psi)] \Big\} \frac{d\psi}{\sin \psi \cos^{11/3} \psi} . \qquad \text{(G4)}$$

Now, η_R is a sum of two integrals of the form appearing on the left side of the stationary phase formula (F12), with

$$\beta(\psi) \frac{1}{\sin \psi \cos^{11} \psi} ,$$

$$f(\psi) = \cos^{2/3} \psi (\tau \cos \psi + \sin \psi)$$

The points of stationary phase are easily calculated to be the points where

$$\cos^2 \psi_0 = \frac{4 + 5\tau^2 \pm \tau\sqrt{24 + 25\tau^2}}{10(1+\tau^2)} ,$$

and simple reasoning shows that it is only when the upper sign is chosen that ψ_0 lies in the range $0 \le \psi_0 \le \pi/2$. To shorten the notation, we set $q^3 = \cos \psi_0$. Thus, we set

$$q(\tau) = \left[\frac{4 + 5\tau^2 + \tau\sqrt{24 + 25\tau^2}}{10(1+\tau^2)} \right]^{1/6} ,$$

and we let $\tau(q)$ be the inverse of this function. Also, we let

$$\beta(q) = \frac{1}{q^{11}\sqrt{1 - q^6}}\,,$$

$$f(q) = q^5\,\tau(q) + q^2\sqrt{1 - q^6}\,, \qquad \text{(G5)}$$

$q_\pm = q(\tau_\pm)$, $\beta_\pm = \beta(q_\pm)$ and $f_\pm = f(q_\pm)$. Then, a simple calculation shows that

$$f''(q) := \frac{d^2}{d\psi^2} f(q)\bigg|_{\psi=\psi_0} = \frac{5\tau(2-5q^6)}{9q} - \frac{2 + 25q^6}{9q^4}\sqrt{1 - q^6}\,.$$

This is always negative. Thus, using (F12) in (G4), we find

$$\eta_R = \beta_+\sqrt{\frac{2\pi}{\gamma|f_+''|}}\sin\left(\gamma f_+ - \frac{\pi}{4}\right) - \beta_-\sqrt{\frac{2\pi}{\gamma|f_-''|}}\sin\left(\gamma f_- - \frac{\pi}{4}\right)\,. \qquad \text{(G6)}$$

We remind the reader have that, in deriving (G6), we have assumed

$$\gamma = \frac{\varepsilon F^{1/3} b}{\mu h} = \frac{\varepsilon F^{1/3}}{2\mu h}\sqrt{\frac{A}{\alpha}} >> 1\,. \qquad \text{(G7)}$$

We need a formula like (G6) for the vertical force on the ice due to the waves. Now, the vertical component of stress at a point in the ice is $(\eta_{xx}+\eta_{zz})(\sigma y)/(1-\sigma)$. The total force acting at any point on the ice is obtained by integration with respect to y. Thus,

$$\hat{V} = -\frac{\sigma h^2}{2(1-\sigma)}\,k^2\hat{\eta}\,.$$

The same analysis that was used to derive (G6) can now be used again to derive an approximate formula for V. The result is that V is proportional to something having the same form as (G6), but with β given by

$$\beta(q) = -\frac{1}{q^7\sqrt{1 - q^6}}\,, \qquad \text{(G8)}$$

instead of (G5).

Library and Information Centre
Centre de Documentation (CSA)
RECEIVED – REÇU
SEP 10 1984
Department Publication
Transport Canada / Transports Canada